Eur. Phys. J. C 39, 465–481 (2005)
Digital Object Identifier (DOI) 10.1140/epjc/s2005-02112-6

THE EUROPEAN PHYSICAL JOURNAL C

High-precision predictions for the MSSM Higgs sector at $\mathcal{O}(\alpha_b\alpha_s)$

S. Heinemeyer[1,a], W. Hollik[2,b], H. Rzehak[2,c], G. Weiglein[3,d]

[1] CERN TH Division, Department of Physics, 1211 Geneva 23, Switzerland
[2] Max-Planck-Institut für Physik (Werner-Heisenberg-Institut), Föhringer Ring 6, 80805 Munich, Germany
[3] Institute for Particle Physics Phenomenology, University of Durham, Durham DH1 3LE, UK

Received: 12 November 2004 /
Published online: 25 January 2005 –

Abstract. We evaluate $\mathcal{O}(\alpha_b\alpha_s)$ corrections in the Higgs boson sector of the $\mathcal{CP}$-conserving MSSM, generalising the known result in the literature to arbitrary values of $\tan\beta$. A detailed analysis of the renormalisation in the bottom/scalar bottom sector is performed. Concerning the lightest MSSM Higgs boson mass, we find relatively small corrections for positive μ, while for $\mu < 0$ the genuine two-loop $\mathcal{O}(\alpha_b\alpha_s)$ corrections can amount up to 3 GeV. Different renormalisation schemes are applied and numerically compared. It is demonstrated that some care has to be taken in choosing an appropriate renormalisation prescription in order to avoid artificially large corrections. The residual dependence on the renormalisation scale is investigated, and the remaining theoretical uncertainties from unknown higher-order corrections in this sector are discussed for different regions of the MSSM parameter space.

1 Introduction

A crucial prediction of the minimal supersymmetric standard model (MSSM) [1] is the existence of at least one light Higgs boson. The search for this particle is one of the main goals at the present and the next generation of colliders. Direct searches at LEP have already ruled out a considerable fraction of the MSSM parameter space [2, 3], and the forthcoming high-energy experiments at the Tevatron, the LHC, and the International Linear Collider (ILC) will either discover a light Higgs boson or rule out supersymmetry (SUSY) as a viable theory for physics at the weak scale. Furthermore, if one or more Higgs bosons are discovered, bounds on their masses and couplings will be set at the LHC [4–6]. Eventually the masses and couplings will be determined with high accuracy at the ILC [7–9]. Thus, precise knowledge of the dependence of masses and mixing angles in the MSSM Higgs sector on the relevant supersymmetric parameters is of utmost importance to reliably compare the predictions of the MSSM with the (present and future) experimental results.

The status of the available results for the higher-order contributions to the neutral $\mathcal{CP}$-even MSSM Higgs boson masses can be summarised as follows. For the one-loop part, the complete result within the MSSM is known [10–13]. The dominant one-loop contribution is the $\mathcal{O}(\alpha_t)$ term due to top and stop loops ($\alpha_t \equiv h_t^2/(4\pi)$, h_t being the superpotential top coupling). Corrections from the bottom/sbottom sector can also give large effects, in particular for large values of $\tan\beta$, the ratio of the two vacuum expectation values, $\tan\beta = v_2/v_1$. The computation of two-loop corrections is also quite advanced. It has now reached a stage such that all the presumably dominant contributions are known. They include the strong corrections, usually indicated as $\mathcal{O}(\alpha_t\alpha_s)$, and Yukawa corrections, $\mathcal{O}(\alpha_t^2)$, to the dominant one-loop $\mathcal{O}(\alpha_t)$ term, as well as the strong corrections to the bottom/sbottom one-loop $\mathcal{O}(\alpha_b)$ term ($\alpha_b \equiv h_b^2/(4\pi)$), i.e. the $\mathcal{O}(\alpha_b\alpha_s)$ contribution, derived in the limit $\tan\beta \to \infty$. Presently, the $\mathcal{O}(\alpha_t\alpha_s)$ [14–23], $\mathcal{O}(\alpha_t^2)$ [14,15,24,25] and the $\mathcal{O}(\alpha_b\alpha_s)$ [26] contributions to the self-energies are known for vanishing external momenta. Most recently also the corrections $\mathcal{O}(\alpha_t\alpha_b)$ and $\mathcal{O}(\alpha_b^2)$ [27], a "full" two-loop effective potential calculation [28] and an evaluation of the leading two-loop momentum dependent effects [29] have become available. In the (s)bottom corrections the all-order resummation of the $\tan\beta$-enhanced terms, $\mathcal{O}(\alpha_b(\alpha_s\tan\beta)^n)$, is also performed [30,31]. Reviews with further references can be found in [32–34].

The $b/\tilde{b}$ sector has attracted considerable attention in the last years, since its corrections to the MSSM Higgs boson sector have been found to be large in certain parts of the MSSM parameter space, possibly even exceeding the size of the top/stop corrections. This can happen especially for large values of $\tan\beta$ and the supersymmetric Higgs mass parameter μ. For illustration, we show in Fig. 1 the shift in the lightest $\mathcal{CP}$-even Higgs boson mass, ΔM_h, arising from the $b/\tilde{b}$ sector at the one-loop level (all two-loop corrections are omitted here) as a function of the bottom-quark mass for large $\tan\beta$ and $|\mu|$. The bottom-quark mass in this plot is understood to be an effective mass that in-

[a] e-mail: Sven.Heinemeyer@cern.ch
[b] e-mail: hollik@mppmu.mpg.de
[c] e-mail: hr@mppmu.mpg.de
[d] e-mail: Georg.Weiglein@durham.ac.uk

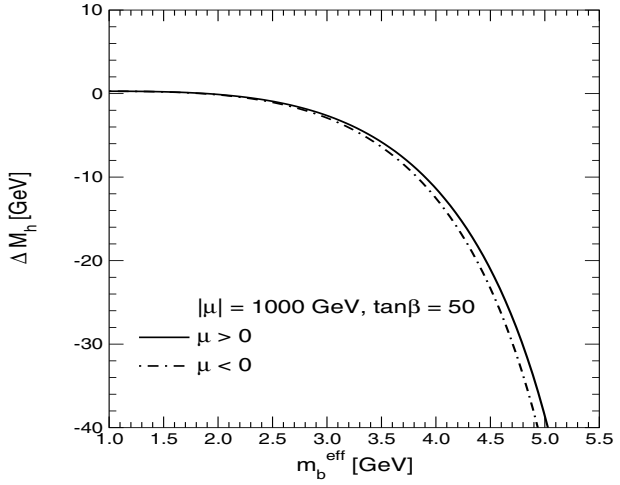

Fig. 1. The shift in the lightest $\mathcal{CP}$-even Higgs boson mass from the one-loop corrections in the $b/\tilde{b}$ sector is shown as a function of the (effective) bottom-quark mass for $\mu = \pm 1000\,\text{GeV}$, $\tan\beta = 50$, $M_{\text{SUSY}} = 600\,\text{GeV}$, $A_t = A_b = 500\,\text{GeV}$, $M_A = 700\,\text{GeV}$

cludes higher-order effects (see the discussion in Sect. 3). The figure demonstrates that corrections from the $b/\tilde{b}$ sector can get large if the effective bottom mass is larger than about 3 GeV.

The possibly large size of the corrections from the $b/\tilde{b}$ sector makes it desirable to investigate the corresponding two-loop corrections and thus to analyse the renormalisation in this sector. An inconvenient choice could give rise to artificially large corrections, whereas a convenient scheme absorbs the dominant contributions into the one-loop result such that higher-order corrections remain small. The comparison of different schemes (where no artificially enhanced corrections appear) gives an indication of the possible size of the missing higher-order terms of $\mathcal{O}(\alpha_b\alpha_s^2)$.

In this paper we derive the result for the $\mathcal{O}(\alpha_b\alpha_s)$ corrections in various renormalisation schemes. The relations between the different parameters in these schemes are worked out in detail. The absorption of leading higher-order contributions into an effective bottom-quark mass is discussed. We perform a numerical analysis of the various schemes and compare our results with a previous evaluation of the $\mathcal{O}(\alpha_b\alpha_s)$ corrections carried out in the limit where $\tan\beta$ is infinitely large [26]. We discuss the dependence of our result on the renormalisation scale and provide an estimate of the remaining theoretical uncertainties in this sector.[1]

This paper is organised as follows: in Sect. 2 we briefly review the MSSM Higgs boson sector, outline the corresponding renormalisation at the two-loop level, and describe the evaluation of the diagrams of $\mathcal{O}(\alpha_b\alpha_s)$. Section 3 contains a detailed description of the renormalisation of the scalar top and scalar bottom sector, which is explicitly carried out in four different renormalisation schemes for the latter. The numerical analysis of the $\mathcal{O}(\alpha_b\alpha_s)$ corrections, the comparison of the different schemes, the investigation of the renormalisation scale, and the comparison with the previous result are performed in Sect. 4. The conclusions can be found in Sect. 5.

2 The Higgs sector at higher orders

We recall that the Higgs sector of the MSSM [35] comprises two neutral $\mathcal{CP}$-even Higgs bosons, h and H ($m_h < m_H$), the $\mathcal{CP}$-odd A boson,[2] and two charged Higgs bosons, $H^\pm$. At the tree level, the masses $m_{h,\text{tree}}$ and $m_{H,\text{tree}}$ can be calculated in terms of M_Z, M_A and $\tan\beta$ from the mass matrix for the neutral $\mathcal{CP}$-even Higgs components (denoted by ϕ):

$$\mathcal{M}_\phi = \tag{1}$$
$$\begin{pmatrix} M_A^2 \sin^2\beta + M_Z^2 \cos^2\beta & -(M_A^2 + M_Z^2)\sin\beta\cos\beta \\ -(M_A^2 + M_Z^2)\sin\beta\cos\beta & M_A^2\cos^2\beta + M_Z^2\sin^2\beta \end{pmatrix},$$

and by diagonalization,

$$\begin{pmatrix} m_{H,\text{tree}}^2 & 0 \\ 0 & m_{h,\text{tree}}^2 \end{pmatrix} = \mathcal{U}_\phi\, \mathcal{M}_\phi\, \mathcal{U}_\phi^\dagger\,,$$
$$\mathcal{U}_\phi = \begin{pmatrix} \cos\alpha & \sin\alpha \\ -\sin\alpha & \cos\alpha \end{pmatrix}, \tag{2}$$

with the angle α determined by

$$\tan 2\alpha = \tan 2\beta\, \frac{M_A^2 + M_Z^2}{M_A^2 - M_Z^2}, \quad -\frac{\pi}{2} < \alpha < 0. \tag{3}$$

In the Feynman diagram (FD) approach, the higher-order corrected Higgs boson masses, M_h and M_H, are derived as the poles of the h, H-propagator matrix, i.e. by solving the equation

$$\left[p^2 - m_{h,\text{tree}}^2 + \hat{\Sigma}_{hh}(p^2)\right]\left[p^2 - m_{H,\text{tree}}^2 + \hat{\Sigma}_{HH}(p^2)\right] - \left[\hat{\Sigma}_{hH}(p^2)\right]^2 = 0\,. \tag{4}$$

The renormalised self-energies

$$\hat{\Sigma}(p^2) = \begin{pmatrix} \hat{\Sigma}_{HH}(p^2) & \hat{\Sigma}_{hH}(p^2) \\ \hat{\Sigma}_{hH}(p^2) & \hat{\Sigma}_{hh}(p^2) \end{pmatrix} \tag{5}$$

can be expanded according to the one-, two-, ... loop-order contributions,

$$\hat{\Sigma}(p^2) = \hat{\Sigma}^{(1)}(p^2) + \hat{\Sigma}^{(2)}(p^2) + \ldots\,. \tag{6}$$

The dominant one-loop contributions to the Higgs boson self-energies (and thus to the Higgs boson masses) from the $b/\tilde{b}$ sector are of $\mathcal{O}(\alpha_b)$ and arise from the Yukawa part of the theory (neglecting the gauge couplings) evaluated at $p^2 = 0$. This has been verified by comparison with the full one-loop result from the $b/\tilde{b}$ sector. Hence, the leading two-loop

[1] This kind of issues have not been addressed in [28, 29].

[2] Throughout this paper we assume that $\mathcal{CP}$ is conserved.

corrections from the $b/\tilde{b}$ sector are the $\mathcal{O}(\alpha_s)$ corrections to those dominant one-loop contributions; they are obtained in the same limit, i.e. for zero external momentum and neglecting the gauge couplings (the same approximations have been made in [26]). This approach is analogous to the way the leading one- and two-loop contributions in the top/stop sector have been obtained, see e.g. [19].

The renormalisation of the Higgs boson mass matrix for the $\mathcal{O}(\alpha_b\alpha_s)$ corrections under consideration follows the description for the $\mathcal{O}(\alpha_t\alpha_s)$ terms given in [19]. Renormalisation can be performed by adding the appropriate counterterms,

$$\mathcal{M}_\phi \to \mathcal{M}_\phi + \delta\mathcal{M}_\phi^{(1)} + \delta\mathcal{M}_\phi^{(2)} + \dots\,, \tag{7}$$

where $\delta\mathcal{M}_\phi^{(i)}$ denotes the ith-loop counterterm matrix consisting of the counterterms to the parameters in the tree-level mass matrix (1). Field renormalisation is not needed for the leading $\mathcal{O}(\alpha_b\alpha_s)$ corrections. The renormalised two-loop Higgs boson self-energies with the leading contributions of $\mathcal{O}(\alpha_b\alpha_s)$ are thus given by

$$\hat{\Sigma}^{(2)}(0) = \Sigma^{(2)}(0) - \mathcal{U}_\phi \delta\mathcal{M}_\phi^{(2)} \mathcal{U}_\phi^\dagger\,. \tag{8}$$

The counterterm matrix in (8) is composed of the counterterms for the A boson mass and for the tadpoles $t_{h,H}$ (with $s_\mathrm{W} \equiv \sin\theta_\mathrm{W}$, $c_\mathrm{W} = \cos\theta_\mathrm{W}$),

$$\begin{aligned}
\delta\mathcal{M}_\phi^{(2)} = {} & \begin{pmatrix} \sin^2\beta & -\sin\beta\cos\beta \\ -\sin\beta\cos\beta & \cos^2\beta \end{pmatrix} \delta M_A^{2\,(2)} \\
& + \frac{e}{2M_Z c_\mathrm{W} s_\mathrm{W}} \begin{pmatrix} -\cos\beta(1+\sin^2\beta) & -\sin^3\beta \\ -\sin^3\beta & \cos\beta\sin^2\beta \end{pmatrix} \\
& \times(\cos\alpha\,\delta t_H^{(2)} - \sin\alpha\,\delta t_h^{(2)}) \\
& + \frac{e}{2M_Z c_\mathrm{W} s_\mathrm{W}} \begin{pmatrix} \cos^2\beta\sin\beta & -\cos^3\beta \\ -\cos^3\beta & -(1+\cos^2\beta)\sin\beta \end{pmatrix} \\
& \times(\sin\alpha\,\delta t_H^{(2)} + \cos\alpha\,\delta t_h^{(2)})\,.
\end{aligned} \tag{9}$$

The counterterms are determined by the following conditions.

(i) On-shell renormalisation of the A boson mass, formulated in the approximation of vanishing external momentum, determines the two-loop A-mass counterterm $\delta M_A^{2\,(2)}$ according to

$$\delta M_A^{2\,(2)} = \Sigma_{AA}^{(2)}(0)\,. \tag{10}$$

(ii) Tadpole renormalisation determines the tadpole counterterms by the requirements

$$\delta t_H^{(2)} = -t_H^{(2)}\,, \quad \delta t_h^{(2)} = -t_h^{(2)}\,, \tag{11}$$

which means that the minimum of the Higgs potential is not shifted.

The genuine two-loop Feynman diagrams to be evaluated for the Higgs boson self-energies and the tadpoles are shown Figs. 2 and 3. The diagrams with sub-loop renormalisation are depicted in Figs. 4 and 5. The counterterms for the insertions, where different renormalisation schemes will be investigated, are specified in the next section.

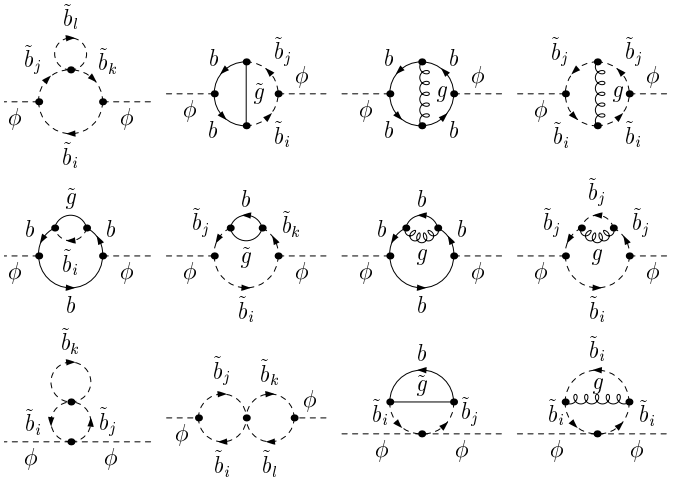

Fig. 2. Generic two-loop diagrams for the Higgs boson self-energies ($\phi = h, H, A$; $i, j, k, l = 1, 2$)

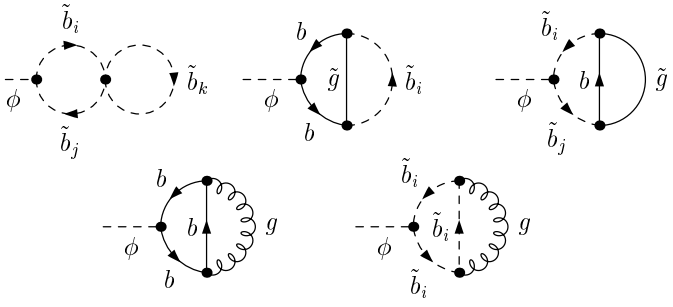

Fig. 3. Generic two-loop diagrams for the Higgs tadpoles ($\phi = h, H$; $i, j, k = 1, 2$)

The diagrams and the corresponding amplitudes have been generated with the package FeynArts [36,37]. The further evaluation has been done using the program TwoCalc

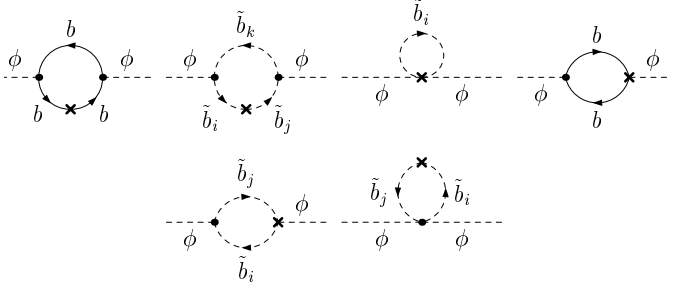

Fig. 4. Generic one-loop diagrams with counterterm insertion for the Higgs boson self-energies ($\phi = h, H, A$, $i, j, k = 1, 2$)

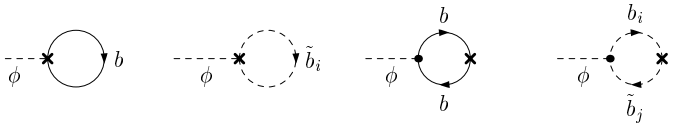

Fig. 5. Generic one-loop diagrams with counterterm insertion for the Higgs tadpoles ($\phi = h, H$, $i, j = 1, 2$)

[38]. The resulting expressions are given in terms of the one-loop functions A_0 and B_0 [39], and the two-loop vacuum integrals [40].

3 Renormalisation of the quark/squark sector

Since the two-loop self-energy is considered at $\mathcal{O}(\alpha_{\{t,b\}}\alpha_s)$ it is sufficient to determine the counterterms induced by the strong interaction only.

The squark-mass terms of the Lagrangian, for a given species of squarks $\tilde{q}$, can be written as the bilinear expression

$$\mathcal{L}_{\tilde{q}-\text{mass}} = -\left(\tilde{q}_{\text{L}}^{\dagger}, \tilde{q}_{\text{R}}^{\dagger}\right) \mathcal{M}_{\tilde{q}} \begin{pmatrix} \tilde{q}_{\text{L}} \\ \tilde{q}_{\text{R}} \end{pmatrix}, \tag{12}$$

with $\mathcal{M}_{\tilde{q}}$ as the squark-mass matrix squared,

$$\mathcal{M}_{\tilde{q}} = \tag{13}$$
$$\begin{pmatrix} M_{\text{L}}^2 + m_q^2 + M_Z^2 c_{2\beta}(T_q^3 - Q_q s_{\text{W}}^2) & m_q(A_q - \mu\kappa) \\ m_q(A_q - \mu\kappa) & M_{\tilde{q}_{\text{R}}}^2 + m_q^2 + M_Z^2 c_{2\beta} Q_q s_{\text{W}}^2 \end{pmatrix},$$

where the quantities M_{L}^2, $M_{\tilde{q}_{\text{R}}}^2$, A_q are soft-breaking parameters, and μ is the supersymmetric Higgs mass parameter. Since we are dealing in this paper with a $\mathcal{CP}$-conserving Higgs sector, these parameters are treated as real. As an abbreviation, $c_{2\beta} \equiv \cos(2\beta)$ is introduced; κ is defined as $\kappa = \cot\beta$ for *up*-type squarks and $\kappa = \tan\beta$ for *down*-type squarks. m_q, Q_q, and T_q^3 are mass, charge, and isospin of the quark q.

The mass matrix (13) can be diagonalised by a unitary transformation, which in our case of real parameters involves a mixing angle $\theta_{\tilde{q}}$,

$$\begin{pmatrix} \tilde{q}_1 \\ \tilde{q}_2 \end{pmatrix} = \mathcal{U}_{\tilde{q}} \begin{pmatrix} \tilde{q}_{\text{L}} \\ \tilde{q}_{\text{R}} \end{pmatrix},$$
$$\mathcal{U}_{\tilde{q}} = \begin{pmatrix} U_{\tilde{q}_{11}} & U_{\tilde{q}_{12}} \\ U_{\tilde{q}_{21}} & U_{\tilde{q}_{22}} \end{pmatrix} = \begin{pmatrix} \cos\theta_{\tilde{q}} & \sin\theta_{\tilde{q}} \\ -\sin\theta_{\tilde{q}} & \cos\theta_{\tilde{q}} \end{pmatrix}. \tag{14}$$

In the $(\tilde{q}_1, \tilde{q}_2)$-basis, the squared-mass matrix is diagonal,

$$\mathcal{D}_{\tilde{q}} = \mathcal{U}_{\tilde{q}} \mathcal{M}_{\tilde{q}} \mathcal{U}_{\tilde{q}}^{\dagger} = \begin{pmatrix} m_{\tilde{q}_1}^2 & 0 \\ 0 & m_{\tilde{q}_2}^2 \end{pmatrix}, \tag{15}$$

with the eigenvalues $m_{\tilde{q}_1}^2$ and $m_{\tilde{q}_2}^2$ given by

$$m_{\tilde{q}_{1,2}}^2 = \frac{1}{2}(M_{\text{L}}^2 + M_{\tilde{q}_{\text{R}}}^2) + m_q^2 + \frac{1}{2} T_q^3 M_Z^2 c_{2\beta}$$
$$\pm \frac{1}{2} \frac{M_{\text{L}}^2 - M_{\tilde{q}_{\text{R}}}^2 + M_Z^2 c_{2\beta}(T_q^3 - 2Q_q s_{\text{W}}^2)}{|M_{\text{L}}^2 - M_{\tilde{q}_{\text{R}}}^2 + M_Z^2 c_{2\beta}(T_q^3 - 2Q_q s_{\text{W}}^2)|}$$
$$\times \Big(\left[M_{\text{L}}^2 - M_{\tilde{q}_{\text{R}}}^2 + M_Z^2 c_{2\beta}(T_q^3 - 2Q_q s_{\text{W}}^2)\right]^2$$
$$+ 4 m_q^2 (A_q - \mu\kappa)^2 \Big)^{1/2}. \tag{16}$$

The squark-mass matrix can now be expressed in terms of the two mass eigenvalues and the mixing angle, yielding

$$\mathcal{M}_{\tilde{q}} = \tag{17}$$
$$\begin{pmatrix} \cos^2\theta_{\tilde{q}}\, m_{\tilde{q}_1}^2 + \sin^2\theta_{\tilde{q}}\, m_{\tilde{q}_2}^2 & \sin\theta_{\tilde{q}}\cos\theta_{\tilde{q}}\,(m_{\tilde{q}_1}^2 - m_{\tilde{q}_2}^2) \\ \sin\theta_{\tilde{q}}\cos\theta_{\tilde{q}}\,(m_{\tilde{q}_1}^2 - m_{\tilde{q}_2}^2) & \sin^2\theta_{\tilde{q}}\, m_{\tilde{q}_1}^2 + \cos^2\theta_{\tilde{q}}\, m_{\tilde{q}_2}^2 \end{pmatrix}.$$

3.1 Renormalisation of the top and scalar top sector

The $(t, \tilde{t})$ sector contains four independent parameters: the top-quark mass m_t, the stop masses $m_{\tilde{t}_1}$ and $m_{\tilde{t}_2}$, and either the squark mixing angle $\theta_{\tilde{t}}$ or, equivalently, the trilinear coupling A_t. Accordingly, the renormalisation of this sector is performed by introducing four counterterms that are determined by four independent renormalisation conditions.

The following renormalisation conditions are imposed (the procedure is equivalent to that of [41], although there no reference is made to the mixing angle).
(i) On-shell renormalisation of the top-quark mass yields the top mass counterterm,

$$\delta m_t = \frac{1}{2} m_t \left[\text{Re}\,\Sigma_{t_{\text{L}}}(m_t^2) + \text{Re}\,\Sigma_{t_{\text{R}}}(m_t^2) + 2\,\text{Re}\,\Sigma_{t_S}(m_t^2)\right], \tag{18}$$

with the scalar coefficients of the unrenormalised top-quark self-energy, $\Sigma_t(p)$, in the Lorentz decomposition

$$\Sigma_t(p) = \not{p}\omega_- \Sigma_{t_{\text{L}}}(p^2) + \not{p}\omega_+ \Sigma_{t_{\text{R}}}(p^2) + m_t \Sigma_{t_S}(p^2). \tag{19}$$

(ii) On-shell renormalisation of the stop masses determines the mass counterterms

$$\delta m_{\tilde{t}_1}^2 = \text{Re}\,\Sigma_{\tilde{t}_{11}}(m_{\tilde{t}_1}^2), \quad \delta m_{\tilde{t}_2}^2 = \text{Re}\,\Sigma_{\tilde{t}_{22}}(m_{\tilde{t}_2}^2), \tag{20}$$

in terms of the diagonal squark self-energies.
(iii) The counterterm for the mixing angle, $\theta_{\tilde{t}}$ (entering (17)), is fixed in the following way:

$$\delta\theta_{\tilde{t}} = \frac{\text{Re}\,\Sigma_{\tilde{t}_{12}}(m_{\tilde{t}_1}^2) + \text{Re}\,\Sigma_{\tilde{t}_{12}}(m_{\tilde{t}_2}^2)}{2(m_{\tilde{t}_1}^2 - m_{\tilde{t}_2}^2)}, \tag{21}$$

involving the non-diagonal squark self-energy. (This is a convenient choice for the treatment of $\mathcal{O}(\alpha_s)$ corrections. If electroweak contributions were included, a manifestly gauge-independent definition would be more appropriate.)

In the renormalised vertices with squark and Higgs fields, the counterterm of the trilinear coupling A_t appears. Having already specified $\delta\theta_{\tilde{t}}$, the A_t counterterm cannot be defined independently but follows from the relation

$$\sin 2\theta_{\tilde{t}} = \frac{2m_t(A_t - \mu\cot\beta)}{m_{\tilde{t}_1}^2 - m_{\tilde{t}_2}^2}, \tag{22}$$

yielding

$$\delta A_t = \frac{1}{m_t} \left[\frac{1}{2}\sin 2\theta_{\tilde{t}} \left(\delta m_{\tilde{t}_1}^2 - \delta m_{\tilde{t}_2}^2\right)\right.$$

Table 1. Summary of the four renormalisation schemes for the bottom-quark/squark sector investigated below. Blank entries indicate dependent quantities

Scheme	$m^2_{\tilde{b}_2}$	m_b	A_b	$\theta_{\tilde{b}}$
analogous to $t/\tilde{t}$ sector ("m_b OS")	on-shell	on-shell		on-shell
$\overline{\rm DR}$ bottom-quark mass ("m_b $\overline{\rm DR}$")	on-shell	$\overline{\rm DR}$	$\overline{\rm DR}$	
$\overline{\rm DR}$ mixing angle and A_b ("A_b, $\theta_{\tilde{b}}$ $\overline{\rm DR}$")	on-shell		$\overline{\rm DR}$	$\overline{\rm DR}$
on-shell mixing angle and A_b ("A_b, $\theta_{\tilde{b}}$ OS")	on-shell		on-shell	on-shell

$$+\cos 2\theta_{\tilde{t}}(m^2_{\tilde{t}_1}-m^2_{\tilde{t}_2})\,\delta\theta_{\tilde{t}} - \frac{1}{2m_t}\sin 2\theta_{\tilde{t}}(m^2_{\tilde{t}_1}-m^2_{\tilde{t}_2})\,\delta m_t\Big]\,. \quad (23)$$

This relation is valid at $\mathcal{O}(\alpha_s)$ since both μ and $\tan\beta$ do not receive one-loop contributions from the strong interaction.

3.2 Renormalisation of the bottom and scalar bottom sector

Because of SU(2)-invariance the soft-breaking parameters for the left-handed *up*- and *down*-type squarks are identical, and thus the squark masses of a given generation are not independent. The stop and sbottom masses are connected via the relation

$$\cos^2\theta_{\tilde{b}} m^2_{\tilde{b}_1} + \sin^2\theta_{\tilde{b}} m^2_{\tilde{b}_2} = \cos^2\theta_{\tilde{t}} m^2_{\tilde{t}_1} + \sin^2\theta_{\tilde{t}} m^2_{\tilde{t}_2} + m_b^2 - m_t^2 - M_W^2\cos(2\beta)\,, \quad (24)$$

with the entries of the rotation matrix in (14). Since the stop masses have already been renormalised on-shell, only one of the sbottom mass counterterms can be determined independently. In the following, the $\tilde{b}_2$ mass is chosen[3] as the pole mass yielding the counterterm from an on-shell renormalisation condition, i.e.

$$\delta m^2_{\tilde{b}_2} = \mathrm{Re}\,\Sigma_{\tilde{b}_{22}}(m^2_{\tilde{b}_2})\,, \quad (25)$$

whereas the counterterm for $m_{\tilde{b}_1}$ is determined as a combination of other counterterms, according to

$$\delta m^2_{\tilde{b}_1} = \frac{1}{\cos^2\theta_{\tilde{b}}}\Big(\cos^2\theta_{\tilde{t}}\delta m^2_{\tilde{t}_1} + \sin^2\theta_{\tilde{t}}\delta m^2_{\tilde{t}_2} - \sin^2\theta_{\tilde{b}}\delta m^2_{\tilde{b}_2} - \sin 2\theta_{\tilde{t}}(m^2_{\tilde{t}_1}-m^2_{\tilde{t}_2})\delta\theta_{\tilde{t}} + \sin 2\theta_{\tilde{b}}(m^2_{\tilde{b}_1}-m^2_{\tilde{b}_2})\delta\theta_{\tilde{b}} - 2m_t\,\delta m_t + 2m_b\,\delta m_b\Big)\,. \quad (26)$$

Accordingly, the numerical value of $m_{\tilde{b}_1}$ does not correspond to the pole mass. The pole mass can be obtained from $m_{\tilde{b}_1}$ via a finite shift of $\mathcal{O}(\alpha_s)$ (see e.g. [42]).

There are three more parameters with counterterms to be determined: the b-quark mass m_b, the mixing angle $\theta_{\tilde{b}}$, and the trilinear coupling A_b. They are connected via

$$\sin 2\theta_{\tilde{b}} = \frac{2m_b(A_b-\mu\tan\beta)}{m^2_{\tilde{b}_1}-m^2_{\tilde{b}_2}}\,, \quad (27)$$

which reads in terms of counterterms

$$2\cos 2\theta_{\tilde{b}}\,\delta\theta_{\tilde{b}} = \sin 2\theta_{\tilde{b}}\frac{\delta m_b}{m_b} + \frac{2m_b\,\delta A_b}{m^2_{\tilde{b}_1}-m^2_{\tilde{b}_2}} - \sin 2\theta_{\tilde{b}}\frac{\delta m^2_{\tilde{b}_1}-\delta m^2_{\tilde{b}_2}}{m^2_{\tilde{b}_1}-m^2_{\tilde{b}_2}}\,. \quad (28)$$

Only two of the three counterterms, δm_b, $\delta\theta_{\tilde{b}}$, δA_b can be treated as independent, which offers a variety of choices. In the following, four different renormalisation schemes, see Table 1, will be investigated. Two of them are on-shell schemes in the sense that the Higgs self-energies do not depend on the renormalisation scale $\mu^{\overline{\rm DR}}$.

The schemes are described in the following subsections, prior to the discussion of their quantitative numerical features in Sect. 4.

3.2.1 Analogous to the top-quark/squark sector

A straight-forward possibility is to impose renormalisation conditions in analogy to those of the top-quark/squark sector in Sect. 3.1.
(i) On-shell renormalisation of the bottom-quark mass m_b determines the corresponding counterterm as follows:

$$\delta m_b = \frac{1}{2}m_b\left[\mathrm{Re}\,\Sigma_{b_{\rm L}}(m_b^2) + \mathrm{Re}\,\Sigma_{b_{\rm R}}(m_b^2) + 2\,\mathrm{Re}\,\Sigma_{b_S}(m_b^2)\right]\,. \quad (29)$$

(ii) The counterterm for the sbottom mixing angle $\theta_{\tilde{b}}$ is determined in the following way:

$$\delta\theta_{\tilde{b}} = \frac{\mathrm{Re}\,\Sigma_{\tilde{b}_{12}}(m^2_{\tilde{b}_1}) + \mathrm{Re}\,\Sigma_{\tilde{b}_{12}}(m^2_{\tilde{b}_2})}{2(m^2_{\tilde{b}_1}-m^2_{\tilde{b}_2})}\,. \quad (30)$$

The dependent counterterm $\delta m^2_{\tilde{b}_1}$ for the $\tilde{b}_1$ mass is then fully specified by (26). Moreover, A_b is treated here as a dependent quantity; the corresponding counterterm δA_b follows from the relation (28), yielding in combination with (26) the expression

$$\delta A_b = \frac{1}{m_b}\Big[-\tan\theta_{\tilde{b}}\delta m^2_{\tilde{b}_2} + (m^2_{\tilde{b}_1}-m^2_{\tilde{b}_2})\delta\theta_{\tilde{b}} - \delta m_b\left(\frac{1}{2m_b}(m^2_{\tilde{b}_1}-m^2_{\tilde{b}_2})\sin 2\theta_{\tilde{b}} - 2\tan\theta_{\tilde{b}}m_b\right) + \tan\theta_{\tilde{b}}\Big(\cos^2\theta_{\tilde{t}}\delta m^2_{\tilde{t}_1} + \sin^2\theta_{\tilde{t}}\delta m^2_{\tilde{t}_2}$$

[3] This choice is possible since (14)–(16) ensure that the $\tilde{b}_2$ field and the $\tilde{b}_{\rm L}$ field do not coincide.

$$- \sin 2\theta_{\tilde{t}}(m^2_{\tilde{t}_1} - m^2_{\tilde{t}_2})\delta\theta_{\tilde{t}} - 2m_t\delta m_t\Big)\Big] \,. \tag{31}$$

While formally the renormalisation described in this section is the same as in the top/stop sector, there are nevertheless important differences. The top-quark pole mass can be directly extracted from experiment and, due to its large numerical value as compared to other quark masses and the fact that the present experimental error is much larger than the QCD scale, it can be used as input for theory predictions in a well-defined way. For the mass of the bottom quark, on the other hand, problems related to non-perturbative effects are much more severe. Therefore the parameter extracted from the comparison of theory and experiment [43] is not the bottom pole mass. Usually the value of the bottom mass is given in the $\overline{\rm MS}$ renormalisation scheme, with the renormalisation scale $\mu^{\overline{\rm MS}}$ chosen as the bottom-quark mass, i.e. $m_b^{\overline{\rm MS}}(m_b^{\overline{\rm MS}})$ [43].

Another important difference to the top/stop sector is the replacement of $\cot\beta \to \tan\beta$. As will be discussed in more detail below, very large effects can occur in this scheme for large values of μ and $\tan\beta$.

3.2.2 $\overline{\rm DR}$ bottom-quark mass

Potential problems with the bottom pole mass can be avoided by adopting a renormalisation scheme with a running bottom-quark mass. In the context of the MSSM it seems appropriate to use the $\overline{\rm DR}$ scheme [44] and to include the SUSY contributions at $\mathcal{O}(\alpha_s)$ into the running. We therefore choose a scheme where m_b and A_b are both renormalised in the $\overline{\rm DR}$ scheme. The following renormalisation conditions are imposed for the independent quantities.
(i) The b-quark mass is defined in the $\overline{\rm DR}$ scheme, which determines the mass counterterm by the expression

$$\delta m_b = \frac{1}{2} m_b \left[\mathrm{Re}\,\Sigma^{\rm div}_{b_{\rm L}}(m_b^2) + \mathrm{Re}\,\Sigma^{\rm div}_{b_{\rm R}}(m_b^2) + 2\,\mathrm{Re}\,\Sigma^{\rm div}_{b_S}(m_b^2)\right] , \tag{32}$$

where $\Sigma^{\rm div}$ means replacing the one- and two-point integrals A and B_0 in the quark self-energies by their divergent parts in the following way:

$$\begin{aligned} A(m)|_{\rm div} &= m^2 \Delta \,, \\ B_0(p^2, m_1, m_2)|_{\rm div} &= \Delta \,, \end{aligned} \tag{33}$$

with $\Delta = 2/\epsilon - \gamma + \log 4\pi$, and $D = 4 - \epsilon$.
(ii) Besides m_b, also the trilinear coupling A_b is defined within the $\overline{\rm DR}$ scheme. Using (31) and inserting the self-energies yields the counterterm

$$\begin{aligned} \delta A_b = \frac{1}{m_b}\Bigg[& - \tan\theta_{\tilde{b}}\,\mathrm{Re}\,\Sigma^{\rm div}_{\tilde{b}_{22}}(m^2_{\tilde{b}_2}) \\ & + \frac{1}{2}\left(\mathrm{Re}\,\Sigma^{\rm div}_{\tilde{b}_{12}}(m^2_{\tilde{b}_1}) + \mathrm{Re}\,\Sigma^{\rm div}_{\tilde{b}_{12}}(m^2_{\tilde{b}_2})\right) \\ & + \tan\theta_{\tilde{b}}\left(\cos^2\theta_{\tilde{t}}\,\mathrm{Re}\,\Sigma^{\rm div}_{\tilde{t}_{11}}(m^2_{\tilde{t}_1}) + \sin^2\theta_{\tilde{t}}\,\mathrm{Re}\,\Sigma^{\rm div}_{\tilde{t}_{22}}(m^2_{\tilde{t}_2})\right. \\ & \left. - \frac{1}{2}\sin 2\theta_{\tilde{t}}\left(\mathrm{Re}\,\Sigma^{\rm div}_{\tilde{t}_{12}}(m^2_{\tilde{t}_1}) + \mathrm{Re}\,\Sigma^{\rm div}_{\tilde{t}_{12}}(m^2_{\tilde{t}_2})\right)\right) \\ & - m_t^2\left(\mathrm{Re}\,\Sigma^{\rm div}_{t_{\rm L}}(m_t^2) + \mathrm{Re}\,\Sigma^{\rm div}_{t_{\rm R}}(m_t^2) + 2\,\mathrm{Re}\,\Sigma^{\rm div}_{t_S}(m_t^2)\right)\Bigg] \\ & + \frac{1}{2}\left(2\tan\theta_{\tilde{b}} m_b - \frac{1}{2m_b}(m^2_{\tilde{b}_1} - m^2_{\tilde{b}_2})\sin 2\theta_{\tilde{b}}\right) \\ & \times \left(\mathrm{Re}\,\Sigma^{\rm div}_{b_{\rm L}}(m_b^2) + \mathrm{Re}\,\Sigma^{\rm div}_{b_{\rm R}}(m_b^2) + 2\,\mathrm{Re}\,\Sigma^{\rm div}_{b_S}(m_b^2)\right) \,. \end{aligned} \tag{34}$$

The counterterms for the mixing angle, $\delta\theta_{\tilde{b}}$, and the $\tilde{b}_1$ mass, $\delta m^2_{\tilde{b}_1}$, are dependent quantities and can be determined as combinations of the independent counterterms, invoking (26) and (28),

$$\begin{aligned} \delta\theta_{\tilde{b}} = \frac{1}{m^2_{\tilde{b}_1} - m^2_{\tilde{b}_2}}\Bigg[& m_b\delta A_b + \tan\theta_{\tilde{b}}\delta m^2_{\tilde{b}_2} \\ & + \delta m_b\left(\frac{1}{2m_b}(m^2_{\tilde{b}_1} - m^2_{\tilde{b}_2})\sin 2\theta_{\tilde{b}} - 2\tan\theta_{\tilde{b}} m_b\right) \\ & - \tan\theta_{\tilde{b}}\left(\cos^2\theta_{\tilde{t}}\delta m^2_{\tilde{t}_1} + \sin^2\theta_{\tilde{t}}\delta m^2_{\tilde{t}_2}\right. \\ & \left. - \sin 2\theta_{\tilde{t}}\left(m^2_{\tilde{t}_1} - m^2_{\tilde{t}_2}\right)\delta\theta_{\tilde{t}} - 2m_t\delta m_t\right)\Bigg] , \end{aligned} \tag{35}$$

$$\begin{aligned} \delta m^2_{\tilde{b}_1} = & \tan^2\theta_{\tilde{b}}\delta m^2_{\tilde{b}_2} + 2\tan\theta_{\tilde{b}} m_b\delta A_b \\ & + 2\left(\frac{1}{m_b}\sin^2\theta_{\tilde{b}}(m^2_{\tilde{b}_1} - m^2_{\tilde{b}_2}) + (1 - \tan^2\theta_{\tilde{b}})m_b\right)\delta m_b \\ & + (1 - \tan^2\theta_{\tilde{b}})\left(\cos^2\theta_{\tilde{t}}\delta m^2_{\tilde{t}_1} + \sin^2\theta_{\tilde{t}}\delta m^2_{\tilde{t}_2}\right. \\ & \left. - \sin 2\theta_{\tilde{t}}(m^2_{\tilde{t}_1} - m^2_{\tilde{t}_2})\delta\theta_{\tilde{t}} - 2m_t\delta m_t\right) . \end{aligned} \tag{36}$$

The renormalised quantities in this scheme depend on the $\overline{\rm DR}$ renormalisation scale $\mu^{\overline{\rm DR}}$. If not stated otherwise, in all numerical results given in this paper the $\overline{\rm DR}$ scale refers to the top-quark mass, i.e. $\mu^{\overline{\rm DR}} = m_t$.

In order to determine the value of $m_b^{\overline{\rm DR},\rm MSSM}(\mu^{\overline{\rm DR}})$ from the value $m_b^{\overline{\rm MS}}(\mu^{\overline{\rm MS}})$ that is extracted from the experimental data one has to note that by definition $m_b^{\overline{\rm DR},\rm MSSM}$ contains all MSSM contributions at $\mathcal{O}(\alpha_s)$, while $m_b^{\overline{\rm MS}}$ contains only the $\mathcal{O}(\alpha_s)$ SM correction, i.e. the gluon-exchange contribution. Furthermore, a finite shift arises from the transition between the $\overline{\rm MS}$ and the $\overline{\rm DR}$ scheme. As input value for $m_b^{\overline{\rm MS}}(M_Z)$ we use in this paper $m_b^{\overline{\rm MS}}(M_Z) = 2.94\,\mathrm{GeV}$ [45].

The expression for $m_b^{\overline{\rm DR},\rm MSSM}(\mu^{\overline{\rm DR}})$ is most easily derived by formally relating $m_b^{\overline{\rm DR},\rm MSSM}$ to the bottom pole mass first and then expressing the bottom pole mass in terms of the $\overline{\rm MS}$ mass (the large non-perturbative contributions affecting the bottom pole mass drop out in the relation of $m_b^{\overline{\rm DR},\rm MSSM}$ to $m_b^{\overline{\rm MS}}$). Using the equality $m_b^{\rm OS} + \delta m_b^{\rm OS} = m_b^{\overline{\rm DR},\rm MSSM} + \delta m_b^{\overline{\rm DR},\rm MSSM}$ and the expressions for the on-shell counterterm and the $\overline{\rm DR}$ counterterm

given in (29) and (32), respectively, one finds

$$m_b^{\overline{\rm DR},{\rm MSSM}}(\mu^{\overline{\rm DR}}) \quad (37)$$
$$= m_b^{\rm OS} + \frac{1}{2} m_b \left(\Sigma_{b_{\rm L}}^{\rm fin}(m_b{}^2) + \Sigma_{b_{\rm R}}^{\rm fin}(m_b{}^2)\right) + m_b\, \Sigma_{b_S}^{\rm fin}(m_b^2)\,.$$

Here the $\Sigma^{\rm fin}$ are the UV-finite parts of the self-energy coefficients in (29). They depend on the $\overline{\rm DR}$ scale $\mu^{\overline{\rm DR}}$ and are evaluated for on-shell momenta, $p^2 = m_b^2$. Inserting $m_b^{\rm OS} = m_b^{\overline{\rm MS}}(M_Z) b^{\rm shift}$, where

$$b^{\rm shift} \equiv \left[1 + \frac{\alpha_s}{\pi}\left(\frac{4}{3} - \ln\frac{(m_b^{\overline{\rm MS}})^2}{M_Z^2}\right)\right], \quad (38)$$

one finds the desired expression for $m_b^{\overline{\rm DR}}$,

$$m_b^{\overline{\rm DR},{\rm MSSM}}(\mu^{\overline{\rm DR}})$$
$$= m_b^{\overline{\rm MS}}(M_Z) b^{\rm shift} + \frac{1}{2} m_b \left(\Sigma_{b_{\rm L}}^{\rm fin}(m_b{}^2) + \Sigma_{b_{\rm R}}^{\rm fin}(m_b{}^2)\right)$$
$$+ m_b\, \Sigma_{b_S}^{\rm fin}(m_b^2)\,. \quad (39)$$

3.2.3 $\overline{\rm DR}$ mixing angle and A_b

A further possibility is to impose renormalisation conditions for the mixing angle $\theta_{\tilde b}$ and for A_b, and to treat the counterterm of the b-quark mass as a dependent quantity determined as a combination of the other counterterms using the relation (28). The renormalisation conditions in this case read explicitly as follows.
(i) δA_b is determined in the $\overline{\rm DR}$ scheme as in the previous case by the expression (34).
(ii) The mixing angle $\theta_{\tilde b}$, defined in the $\overline{\rm DR}$ scheme, is renormalised by the counterterm

$$\delta\theta_{\tilde b} = \frac{{\rm Re}\,\Sigma_{\tilde b_{12}}^{\rm div}(m_{\tilde b_1}^2) + {\rm Re}\,\Sigma_{\tilde b_{12}}^{\rm div}(m_{\tilde b_2}^2)}{2(m_{\tilde b_1}^2 - m_{\tilde b_2}^2)}\,. \quad (40)$$

The counterterm for the b-quark mass, δm_b, can be obtained using (28) and the constraint (26). It is given by the following quantity (which is well-behaved for $\theta_{\tilde b} \to 0$):

$$\delta m_b = \Big[\tan\theta_{\tilde b}\Big(-\delta m_{\tilde b_2}^2 + \cos^2\theta_{\tilde t}\delta m_{\tilde t_1}^2 + \sin^2\theta_{\tilde t}\delta m_{\tilde t_2}^2$$
$$- \sin 2\theta_{\tilde t}(m_{\tilde t_1}^2 - m_{\tilde t_2}^2)\delta\theta_{\tilde t} - 2m_t\,\delta m_t\Big)$$
$$- m_b\,\delta A_b + (m_{\tilde b_1}^2 - m_{\tilde b_2}^2)\delta\theta_{\tilde b}\Big]$$
$$\times \left[\frac{m_{\tilde b_1}^2 - m_{\tilde b_2}^2}{2m_b}\sin 2\theta_{\tilde b} - 2m_b\tan\theta_{\tilde b}\right]^{-1}. \quad (41)$$

The numerical value of m_b in this scheme is obtained from (39) and the (finite) difference of the counterterms given in (41) and (32).

Finally, (26) yields also the counterterm for the dependent squark mass, $\delta m_{\tilde b_1}^2$, with the specification (41) for the b-mass counterterm.

3.2.4 On-shell mixing angle and A_b

In [26] a renormalisation condition was imposed on the $A\tilde b_1\tilde b_2$ vertex in order to avoid an explicit dependence on the renormalisation scale $\mu^{\overline{\rm DR}}$. For the purpose of comparing our results with those of [26] we include such a renormalisation scheme in our discussion. While in [26] the limit $\tan\beta \to \infty$ has been used to derive all the renormalisation conditions and counterterms, we have derived the relevant quantities for arbitrary values of $\tan\beta$. We call this scheme "on-shell" (as in [26]), although the vertex is taken at an off-shell value of the A boson momentum.

Similarly to the previous scheme, the counterterm for the b-quark mass is derived as a linear combination of other counterterms by means of (28). The independent renormalisation conditions can be formulated as follows.
(i) The counterterm for the mixing angle $\theta_{\tilde b}$ is defined by

$$\delta\theta_{\tilde b} = \frac{{\rm Re}\,\Sigma_{\tilde b_{12}}(m_{\tilde b_1}^2) + {\rm Re}\,\Sigma_{\tilde b_{12}}(m_{\tilde b_2}^2)}{2(m_{\tilde b_1}^2 - m_{\tilde b_2}^2)}\,, \quad (42)$$

as in the scheme "analogous to the top-quark/squark sector".
(ii) A_b is determinded by imposing the condition

$$\hat\Lambda(0, m_{\tilde b_1}^2, m_{\tilde b_1}^2) + \hat\Lambda(0, m_{\tilde b_2}^2, m_{\tilde b_2}^2) = 0\,, \quad (43)$$

with $\hat\Lambda(p_A^2, p_{\tilde b_1}^2, p_{\tilde b_2}^2)$ as the renormalised three-point $A\tilde b_1\tilde b_2$ vertex function,

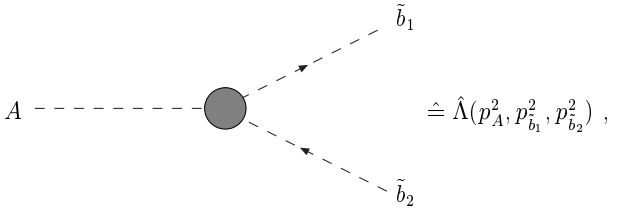

$$\hat\Lambda(p_A^2, p_{\tilde b_1}^2, p_{\tilde b_2}^2) = \Lambda(p_A^2, p_{\tilde b_1}^2, p_{\tilde b_2}^2)$$
$$+ \frac{{\rm i}e}{2M_W\sin\theta_{\rm W}}\Big[m_b\tan\beta\,\delta A_b \quad (44)$$
$$+ (\mu + \tan\beta A_b)\left(\delta m_b + \frac{1}{2}m_b(\delta Z_{\tilde b_1\tilde b_1} + \delta Z_{\tilde b_2\tilde b_2})\right)\Big].$$

In the large-$\tan\beta$ limit, this requirement reproduces the condition applied in [26].

Condition (ii) can be formulated as an equation determining the counterterm for A_b in the following way:

$$\delta A_b$$
$$= {\rm i}\frac{M_W\sin\theta_{\rm W}}{e\, m_b\tan\beta}\left(\Lambda(0, m_{\tilde b_1}^2, m_{\tilde b_1}^2) + \Lambda(0, m_{\tilde b_2}^2, m_{\tilde b_2}^2)\right)$$
$$- \frac{\mu + A_b\tan\beta}{2\tan\beta}(\delta Z_{\tilde b_1\tilde b_1} + \delta Z_{\tilde b_2\tilde b_2})$$
$$+ \frac{\mu + A_b\tan\beta}{m_b\tan\beta}$$

$$
\begin{aligned}
&\times \left[-\mathrm{i}\frac{M_W \sin\theta_W}{e\tan\beta}\left(\Lambda(0,m^2_{\tilde b_1},m^2_{\tilde b_1})+\Lambda(0,m^2_{\tilde b_2},m^2_{\tilde b_2})\right)\right.\\
&+\frac{m_b(\mu+A_b\tan\beta)}{2\tan\beta}(\delta Z_{\tilde b_1\tilde b_1}+\delta Z_{\tilde b_2\tilde b_2})\\
&+(m^2_{\tilde b_1}-m^2_{\tilde b_2})\delta\theta_{\tilde b}\\
&-\tan\theta_{\tilde b}\left(\delta m^2_{\tilde b_2}-\cos^2\theta_{\tilde t}\delta m^2_{\tilde t_1}-\sin^2\theta_{\tilde t}\delta m^2_{\tilde t_2}\right.\\
&\left.\left.+\sin 2\theta_{\tilde t}(m^2_{\tilde t_1}-m^2_{\tilde t_2})\delta\theta_{\tilde t}+2m_t\delta m_t\right)\right]\\
&\times\left[\mu\left(\tan\beta+\frac{1}{\tan\beta}\right)+2m_b\tan\theta_{\tilde b}\right]^{-1}, \qquad (45)
\end{aligned}
$$

where the Z factors are defined as

$$
\delta Z_{\tilde b_i\tilde b_i}=-\frac{\Sigma_{\tilde b_{ii}}(m^2_{\tilde b_1})-\Sigma_{\tilde b_{ii}}(m^2_{\tilde b_2})}{m^2_{\tilde b_1}-m^2_{\tilde b_2}}\,. \qquad (46)
$$

Again, the dependent counterterm for the b-quark mass is determined by (28) and the constraint (26), but now inserting the above specification (45) for δA_b, yielding

$$
\begin{aligned}
&\delta m_b\\
&=-\left[-\mathrm{i}\frac{M_W\sin\theta_W}{e\,\tan\beta}\left(\Lambda(0,m^2_{\tilde b_1},m^2_{\tilde b_1})+\Lambda(0,m^2_{\tilde b_2},m^2_{\tilde b_2})\right)\right.\\
&+\frac{m_b(\mu+A_b\tan\beta)}{2\tan\beta}(\delta Z_{\tilde b_1\tilde b_1}+\delta Z_{\tilde b_2\tilde b_2})\\
&+(m^2_{\tilde b_1}-m^2_{\tilde b_2})\delta\theta_{\tilde b}\\
&+\tan\theta_{\tilde b}\left(-\sin 2\theta_{\tilde t}(m^2_{\tilde t_1}-m^2_{\tilde t_2})\delta\theta_{\tilde t}-\delta m^2_{\tilde b_2}+\cos^2\theta_{\tilde t}\delta m^2_{\tilde t_1}\right.\\
&\left.\left.+\sin^2\theta_{\tilde t}\delta m^2_{\tilde t_2}-2m_t\delta m_t\right)\right]\\
&\times\left[\mu\left(\tan\beta+\frac{1}{\tan\beta}\right)+2m_b\tan\theta_{\tilde b}\right]^{-1}. \qquad (47)
\end{aligned}
$$

The numerical value of m_b in this scheme is obtained from (39) and the (finite) difference of the counterterms given in (47) and (32).

With the specification of δm_b in (47), also the $\tilde b_1$-mass counterterm $\delta m^2_{\tilde b_1}$ in the general relation (26) is fully determined.

3.3 Resummation in the $b/\tilde b$ sector

The relation between the bottom-quark mass and the Yukawa coupling h_b, which in lowest order reads $m_b = h_b v_1/\sqrt{2}$, receives radiative corrections proportional to $h_b v_2 = h_b \tan\beta\, v_1$. Thus, large $\tan\beta$-enhanced contributions can occur, which need to be properly taken into account. As shown in [30, 31] the leading terms of $\mathcal{O}(\alpha_b(\alpha_s\tan\beta)^n)$ can be resummed by using an appropriate effective bottom Yukawa coupling.

Accordingly, an effective bottom-quark mass is obtained by extracting the UV-finite $\tan\beta$-enhanced term Δm_b from (39) (which enters through Σ_{b_S}) and writing it as $1/(1+\Delta m_b)$ into the denominator. In this way the leading powers of $(\alpha_s\tan\beta)^n$ are correctly resummed [30,31]. This yields

$$
\begin{aligned}
&m_b^{\overline{\mathrm{DR}},\mathrm{MSSM}}(\mu^{\overline{\mathrm{DR}}})\\
&=\left(m_b^{\overline{\mathrm{MS}}}(M_Z)b^{\mathrm{shift}}+\frac{1}{2}m_b\left(\Sigma^{\mathrm{fin}}_{b_L}(m_b{}^2)+\Sigma^{\mathrm{fin}}_{b_R}(m_b{}^2)\right)\right.\\
&\qquad\left.+m_b\,\widetilde{\Sigma}^{\mathrm{fin}}_{b_S}(m_b^2)\right)\\
&\quad/(1+\Delta m_b)\,, \qquad (48)
\end{aligned}
$$

where $\widetilde{\Sigma}_{b_S}\equiv\Sigma_{b_S}+\Delta m_b$ denotes the non-enhanced remainder of the scalar b-quark self-energy at $\mathcal{O}(\alpha_s)$, and b^{shift} is given in (38). The $\tan\beta$-enhanced scalar part of the b-quark self-energy, Δm_b, is given at $\mathcal{O}(\alpha_s)$ by[4]

$$
\Delta m_b=\frac{2}{3\pi}\alpha_s\tan\beta\,\mu\,m_{\tilde g}\,I(m^2_{\tilde b_1},m^2_{\tilde b_2},m^2_{\tilde g}), \qquad (49)
$$

with

$$
\begin{aligned}
&I(m^2_{\tilde b_1},m^2_{\tilde b_2},m^2_{\tilde g})\\
&=-\left(m^2_{\tilde b_1}m^2_{\tilde b_2}\log(m^2_{\tilde b_2}/m^2_{\tilde b_1})+m^2_{\tilde b_1}m^2_{\tilde g}\log(m^2_{\tilde b_1}/m^2_{\tilde g})\right.\\
&\qquad\left.+m^2_{\tilde g}m^2_{\tilde b_2}\log(m^2_{\tilde g}/m^2_{\tilde b_2})\right)\\
&\quad\Big/\left((m^2_{\tilde b_1}-m^2_{\tilde g})(m^2_{\tilde g}-m^2_{\tilde b_2})(m^2_{\tilde b_2}-m^2_{\tilde b_1})\right), \qquad (50)
\end{aligned}
$$

and $\Delta m_b > 0$ for $\mu > 0$.

In the "m_b $\overline{\mathrm{DR}}$" scheme we use the effective bottom-quark mass as given in (48) everywhere instead of the $\overline{\mathrm{DR}}$ bottom quark mass (in particular, we use this bottom mass in the sbottom-mass matrix squared, (13), from which the sbottom mass eigenvalues are determined). The numerical values of the bottom-quark mass in the other renormalisation schemes can be obtained from (48) as explained above, and from (51) below.

We incorporate the effective bottom-quark mass of (48) (or the correspondingly shifted value in the other renormalisation schemes) into our one-loop results for the renormalised Higgs boson self-energies, which determine the Higgs boson masses at one-loop order according to (4)–(6). In this way the leading effects of $\mathcal{O}(\alpha_b\alpha_s)$ are absorbed into the one-loop result. We refer to the genuine two-loop contributions, which go beyond this improved one-loop result, as "subleading $\mathcal{O}(\alpha_b\alpha_s)$ corrections" in the following.

[4] There are also corrections of $\mathcal{O}(\alpha_t)$ to Δm_b that can be resummed [31]. These effects usually amount up to 5–10% of the $\mathcal{O}(\alpha_s)$ corrections. Since in this paper we are interested only in the $\mathcal{O}(\alpha_b\alpha_s)$ contributions to the MSSM Higgs sector, these corrections have been neglected. Further corrections from subleading resummation terms can be found in [46].

Table 2. Set of default input parameters

SM parameters:		
$m_t = 174.3\,\text{GeV}$,	$m_b^{\overline{\text{MS}}}(M_Z) = 2.94\,\text{GeV}$,	
$M_Z = 91.1875\,\text{GeV}$,	$M_W = 80.426\,\text{GeV}$,	$G_\text{F} = 1.16639\ 10^{-5}$
parameters of the Higgs sector:		
$M_A = 120\,\text{GeV}$	$\tan\beta = 50$	$\mu = -1000\,\text{GeV}$
soft-breaking parameters:		
for the gauginos:	for the sfermions:	
$M_1 = \frac{5}{3}\frac{\sin^2\theta_\text{W}}{\cos^2\theta_\text{W}} M_2$	$M_\text{L} = M_{L_{\{\tilde{q}_i,\,\tilde{l}_i\}}} = 1000\,\text{GeV}$ with $i = 1, 2, 3$	
$M_2 = 100\,\text{GeV}$	$M_{\tilde{f}_\text{R}} = 1000\,\text{GeV}$ with $f = u, c, t, d, s, b, e, \mu, \tau$	
$M_3 = 1000\,\text{GeV}$	$A_{\{u,c,t\}} = A_{\{d,s,b\}} = A_{\{e,\mu,\tau\}} = 2000\,\text{GeV}$	

4 Numerical results

4.1 Evaluation

If not mentioned explicitly in the text the default set of parameters shown in Table 2 is used. Large values of $\tan\beta$ and $|\mu|$ are chosen in order to illustrate possibly large effects in the $b/\tilde{b}$ sector.

We will mostly discuss the case of negative μ, since according to (48)–(50) this sign of μ leads to a negative Δm_b and therefore to an increase of the effective bottom-quark mass. This gives rise to an enhancement of the corrections from the $b/\tilde{b}$ sector; see Fig. 1. While the negative sign of μ is disfavoured from the comparison of the MSSM prediction [47,48] with the experimental data on the anomalous magnetic moment of the muon [49], it would seem premature at this stage to completely disregard this possibility. For $\mu > 0$, on the other hand, the corrections to the Higgs-boson masses from the $b/\tilde{b}$ sector will normally not exceed the GeV level if the result is expressed in terms of an appropriately chosen running bottom-quark mass (see Fig. 1). It should be noted, however, that the prospective experimental accuracy on M_h at the LHC and the ILC will be significantly below the GeV level, so that the inclusion of non-enhanced two-loop corrections will be necessary in order to achieve the same level of precision for the theoretical prediction (see the discussion below).

For the calculation of the Higgs boson masses presented below the complete one-loop self-energies have been used, with $\tan\beta$ renormalised in the $\overline{\text{DR}}$ scheme [50–52] and with the Z boson mass on-shell. At the two-loop level, besides the $\mathcal{O}(\alpha_b\alpha_s)$ corrections also the contributions $\mathcal{O}(\alpha_t\alpha_s)$ using the one-loop sub-renormalisation of Sect. 3.1 have been included. For simplicity we have neglected the $\mathcal{O}(\alpha_t^2)$ terms [25]. For the $\mathcal{O}(\alpha_t\alpha_s)$ corrections the top pole mass, $m_t = 174.3\,\text{GeV}$, has been used. The inclusion of all known corrections and the new experimental top-quark mass value of $m_t = 178.0\,\text{GeV}$ [53] in our analysis would yield an increase in M_h of $\mathcal{O}(8\,\text{GeV})$ [32]. Therefore the mass values given in our numerical analysis should not be viewed as predictions of M_h; they are rather illustrations of the α_s corrections to the bottom Yukawa contributions at the two-loop level. (It should be noted that the chosen parameters are such that they are not in conflict with the experimental lower bounds on M_h [2,3].)

4.2 Comparison of the different renormalisation schemes

In order to compare the different renormalisation schemes, the parameters entering the one-loop result have to be transformed according to the different renormalisation prescriptions. As our default for which the input parameters are fixed we have chosen the "m_b $\overline{\text{DR}}$" scheme, where m_b and A_b are defined as $\overline{\text{DR}}$ parameters. As explained in Sect. 3, the parameters are converted to a different renormalisation scheme RS (with counterterms δx^RS) with the help of the following transformations:

$$m_b^\text{RS} = m_b^{\overline{\text{DR}}} - \delta m_b^\text{RS}|_\text{finite}\,, \tag{51}$$

$$A_b^\text{RS} = A_b^{\overline{\text{DR}}} - \delta A_b^\text{RS}|_\text{finite}\,, \tag{52}$$

and analogously for the other parameters. If not stated otherwise, the $\overline{\text{DR}}$ scale has always been chosen as $\mu^{\overline{\text{DR}}} = m_t$. As an example, in Tables 3 and 4 numerical values for the bottom-quark mass, A_b and the sbottom masses in the different schemes (see Table 1), are shown for $\tan\beta = 30$ and $\tan\beta = 50$ and using the default values given in Table 2 otherwise.

The values given in Tables 3 and 4 indicate that the "m_b OS" scheme leads to huge corrections in A_b that invalidate the applicability of this scheme. The other schemes give rise to only moderate shifts in the parameters.

The reason for the problematic behaviour of the "m_b OS" scheme is easy to understand. The renormalisation

Table 3. Values of the bottom-quark mass, A_b and $m_{\tilde{b}_1}$ in the different schemes for $\tan\beta = 30$ and $\mu = -1000\,\text{GeV}$. The value of $m_{\tilde{b}_2}$, which is renormalised on-shell (see (25)), is the same in all four schemes, $m_{\tilde{b}_2} = 938.44\,\text{GeV}$

Scheme	m_b [GeV]	A_b [GeV]	$m_{\tilde{b}_1}$ [GeV]
m_b $\overline{\text{DR}}$	3.79	2000.00	1059.95
A_b, $\theta_{\tilde{b}}$ $\overline{\text{DR}}$	3.04	2000.00	1039.50
A_b, $\theta_{\tilde{b}}$ OS	2.99	2332.81	1039.04
m_b OS	3.77	−4284.56	1039.25

Table 4. Values of the bottom-quark mass, A_b and $m_{\tilde{b}_1}$ in the different schemes for $\tan\beta = 50$ and $\mu = -1000\,\text{GeV}$. The value of $m_{\tilde{b}_2}$ is the same in all four schemes, $m_{\tilde{b}_2} = 836.48\,\text{GeV}$

Scheme	m_b [GeV]	A_b [GeV]	$m_{\tilde{b}_1}$ [GeV]
m_b $\overline{\text{DR}}$	5.82	2000.00	1142.16
A_b, $\theta_{\tilde{b}}$ $\overline{\text{DR}}$	5.26	2000.00	1117.93
A_b, $\theta_{\tilde{b}}$ OS	5.24	2219.40	1118.02
m_b OS	4.93	6508.12	1122.04

condition in the "m_b OS" scheme is a condition on the sbottom mixing angle $\theta_{\tilde{b}}$ and thus on the combination $(A_b - \mu \tan\beta)$ (see (28)). In parameter regions where $\mu \tan\beta$ is much larger than A_b, the counterterm δA_b receives a very large finite shift when calculated from the counterterm $\delta\theta_{\tilde{b}}$. More specifically, δA_b as given in (31) contains the contribution

$$\delta A_b = \frac{1}{m_b}\left[-\frac{\delta m_b}{2\,m_b}\,(m^2_{\tilde{b}_1} - m^2_{\tilde{b}_2})\sin 2\theta_{\tilde{b}} + \ldots\right]$$
$$= \frac{1}{m_b}\left[-\delta m_b(A_b - \mu\,\tan\beta) + \ldots\right], \qquad (53)$$

that can give rise to very large corrections to A_b. This problem is avoided in the other renormalisation schemes introduced in Table 1, where the renormalisation condition is applied directly to A_b, rather than deriving δA_b from the renormalisation of the mixing angle.

We now turn to the numerical comparison of the different renormalisation schemes. As discussed above, the $\tan\beta$-enhanced terms of $\mathcal{O}(\alpha_b\alpha_s)$ entering via Δm_b have been absorbed into the one-loop result. The meaning of the various curves in the following figures is specified as (see also Table 1)

(1) dashes with dots (black): $\mathcal{O}(\alpha_t\alpha_s)$ with $m_b^{\overline{\rm DR},\rm MSSM}$, results without subleading two-loop $\mathcal{O}(\alpha_b\alpha_s)$ terms;
(2) dot-dash (light blue): "m_b OS" scheme for subleading two-loop $\mathcal{O}(\alpha_b\alpha_s)$ terms;
(3) solid (red): "m_b $\overline{\rm DR}$" scheme for subleading two-loop $\mathcal{O}(\alpha_b\alpha_s)$ terms;
(4) dotted (dark blue): "A_b, $\theta_{\tilde{b}}$ $\overline{\rm DR}$" scheme for subleading two-loop $\mathcal{O}(\alpha_b\alpha_s)$ terms;
(5) dashes with stars (green): "A_b, $\theta_{\tilde{b}}$ OS" scheme for subleading two-loop $\mathcal{O}(\alpha_b\alpha_s)$ terms.

We start our analysis of the different renormalisation schemes by comparing the results for M_h and M_H as a function of $\tan\beta$ in Fig. 6. The other parameters are as given in Table 2. As expected from the discussion of Tables 3 and 4, the "m_b OS" scheme gives rise to artificially large corrections and shows very large deviations from the other schemes for intermediate and large values of $\tan\beta$. This behaviour is even more pronounced for M_H than for M_h, as can be seen in the lower plot of Fig. 6. These extremely large corrections are a consequence of the large contributions to the counterterm of the parameter A_b (see (53)). The Higgs self-energy contribution from virtual sbottoms contains a term proportional to A_b^2. Using as input a value for A_b according to (52), very large contributions proportional to $(\delta A_b)^2$ are introduced. These corrections are more pronounced in Σ_{HH}, where they enter like $(\cos\alpha\, A_b)^2$, than in Σ_{hh}, where they enter like $(\sin\alpha\, A_b)^2$ ($|\alpha| \ll 1$ in our analysis). The unacceptably large contributions to δA_b in the "m_b OS" scheme invalidate a perturbative treatment in this scheme. We therefore discard this scheme in the following and focus our discussion on the other three schemes defined in Table 1.

The other schemes all give similar and numerically well-behaved results, where M_h starts to decrease rapidly with $\tan\beta$ for $\tan\beta \gtrsim 40$. Negative mass squares are reached at

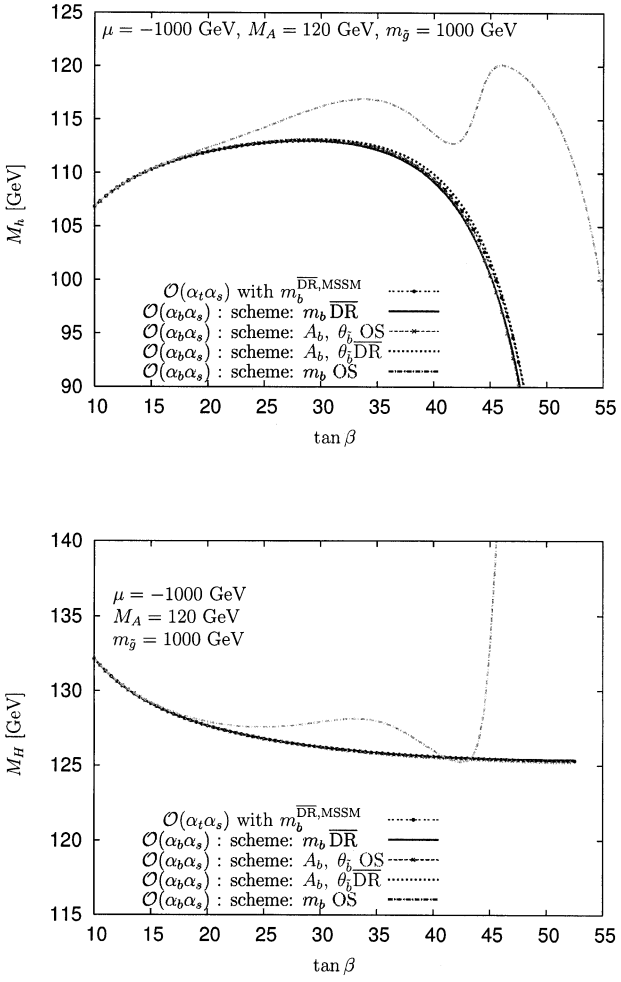

Fig. 6. $\tan\beta$ dependence of M_h and M_H for $M_A = 120\,\text{GeV}$ and μ negative

$\tan\beta \simeq 53$. The main effect comes from the leading contributions of $\mathcal{O}(\alpha_b\alpha_s)$ that enter via the resummation of Δm_b; see (48). The decrease with increasing $\tan\beta$ is mainly due to the dependence of $\Delta m_b \sim \mu\tan\beta$ in (49). The subleading $\mathcal{O}(\alpha_b\alpha_s)$ corrections, which arise from the genuine two-loop diagrams, are of $\mathcal{O}(1\,\text{GeV})$. The differences between the three renormalisation schemes are of similar size. For this particular parameter choice the "A_b, $\theta_{\tilde{b}}$ $\overline{\rm DR}$" scheme enhances M_h, whereas the other two schemes decrease M_h compared to the case where the genuine two-loop corrections are omitted.

In Fig. 7 we show M_h as a function of $\tan\beta$ for the same parameters as in Fig. 6, but with $M_A = 700\,\text{GeV}$. This results in general in larger M_h values, but the general behaviour as a function of $\tan\beta$ is the same as for $M_A = 120\,\text{GeV}$; M_h drops steeply for large $\tan\beta$ values. In all three schemes the subleading terms increase M_h by a few GeV, depending on $\tan\beta$.

As discussed above, large corrections from the $b/\tilde{b}$ sector are only expected for negative values of μ. In Fig. 8 we show the results for M_h as a function of $\tan\beta$ with positive μ and $M_A = 120$ and $700\,\text{GeV}$, respectively. The other parameters are given in Table 2. The positive sign of

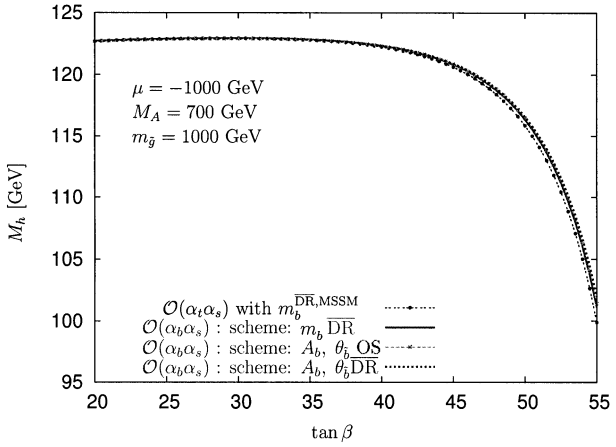

Fig. 7. $\tan\beta$ dependence of M_h for $M_A = 700\,\text{GeV}$ and μ negative

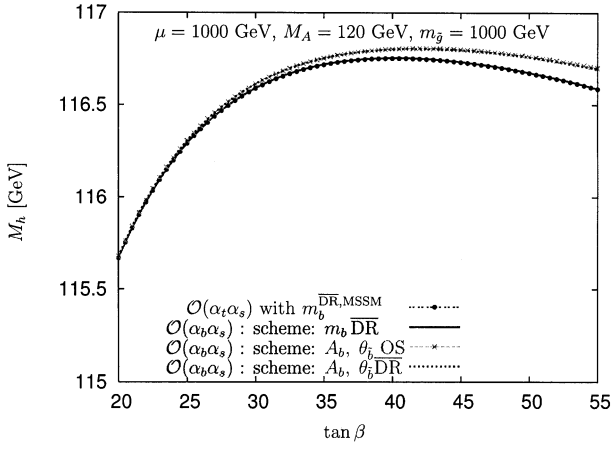

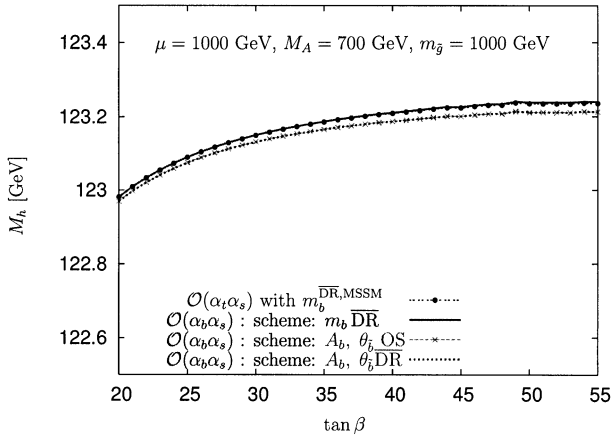

Fig. 8. $\tan\beta$ dependence of M_h for $M_A = 120\,\text{GeV}$ (upper plot) and $M_A = 700\,\text{GeV}$ (lower plot) for positive μ

μ results in a positive Δm_b and thus a smaller numerical value of $m_b^{\overline{\rm DR},\rm MSSM}$. As expected[5], the variation of M_h with $\tan\beta$ is much smaller than for negative μ. Both, the leading corrections, i.e. the $\tan\beta$-enhanced terms of $\mathcal{O}(\alpha_b\alpha_s)$, as well as the subleading corrections are at the level of $\mathcal{O}(100\,\text{MeV})$. The "$m_b\,\overline{\rm DR}$" scheme does not show any visible corrections beyond the resummed contributions. This leads to the conclusion that for positive μ the corrections beyond the one-loop level coming from the $b/\tilde{b}$ sector are sufficiently well under control. However, in view of the fact that the anticipated ILC accuracy on M_h [7–9] and the parametric uncertainty of the theory prediction from the ILC measurement of the top-quark mass [54,55] will both be about 100 MeV, ultimately the aim will be to reduce the theoretical uncertainties from unknown higher-order corrections to at least this level. This will require the inclusion of all two-loop corrections (and a significant part of corrections beyond two-loop order). For the further analysis in this paper we focus on negative values of μ.

[5] See also the discussion in [26], where the opposite sign convention for μ is used.

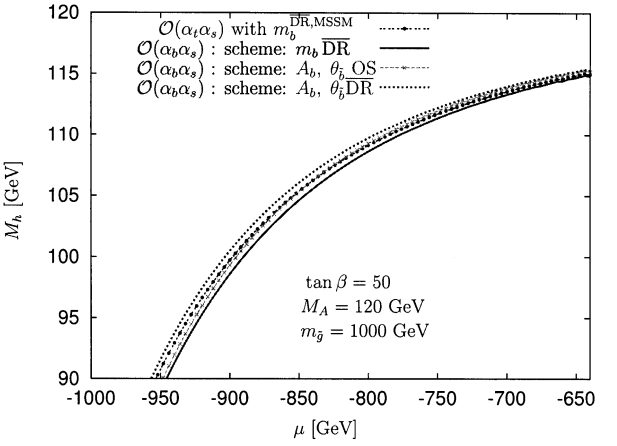

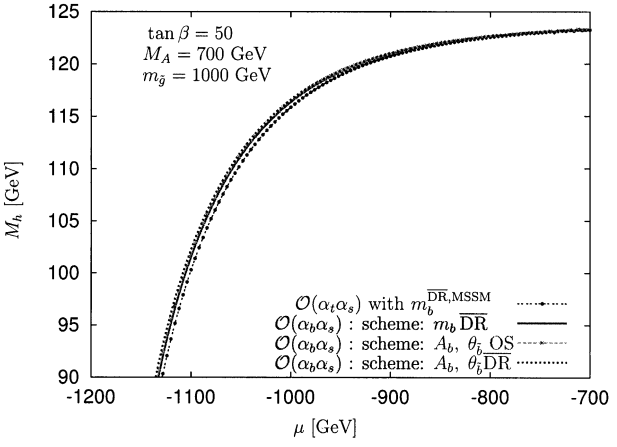

Fig. 9. μ dependence of M_h for $M_A = 120\,\text{GeV}$ (upper plot) and $M_A = 700\,\text{GeV}$ (lower plot) for $\tan\beta = 50$

The variation of M_h with μ (for $\mu < 0$) for $\tan\beta = 50$ is shown in Fig. 9. As can be expected from (49) the corrections at $\mathcal{O}(\alpha_b\alpha_s)$ increase with increasing $|\mu|$. Typically the genuine two-loop contributions are of $\mathcal{O}(1\,\text{GeV})$. For large M_A all the schemes lead to an increase of M_h, whereas for small M_A both negative and positive shifts can occur. Differences in the M_h predictions induced by the differ-

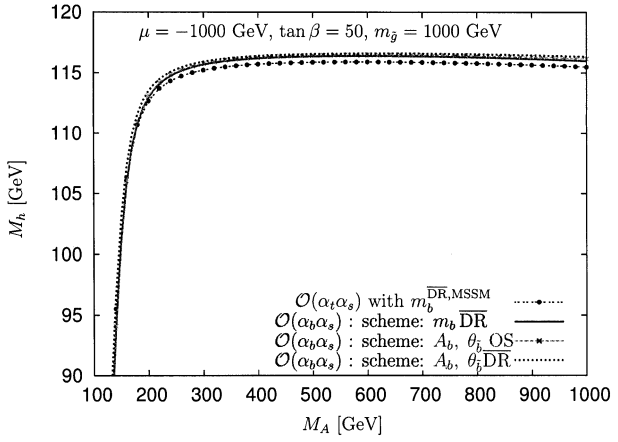

Fig. 10. M_A dependence of M_h for $\tan\beta = 50$ and μ negative

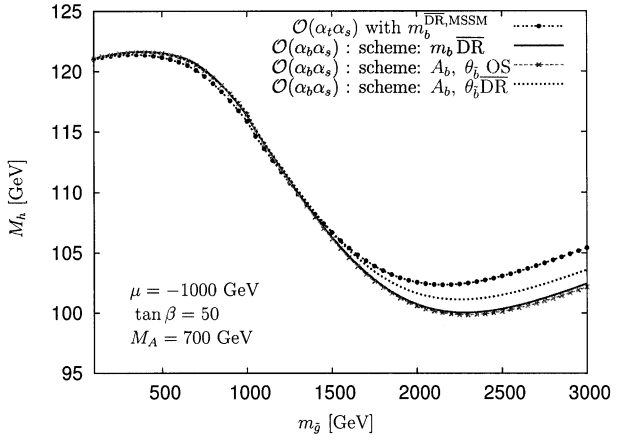

Fig. 11. $m_{\tilde{g}}$ dependence of M_h for $M_A = 700\,\text{GeV}$, $\tan\beta = 50$ and μ negative

ent renormalisation schemes are below the GeV level for large M_A.

In Fig. 10 the dependence of M_h on M_A is shown for the different renormalisation schemes, with the other default parameters from Table 2. For $M_A \gtrsim 200\,\text{GeV}$ the subleading terms of all three schemes enhance M_h by $\mathcal{O}(1\,\text{GeV})$. A decrease only occurs for small values of M_A, depending on the scheme. The differences in the M_h prediction resulting from the use of different renormalisation schemes decrease for $M_A \gtrsim 200\,\text{GeV}$ to $\mathcal{O}(0.1\ \text{GeV})$.

In Fig. 11 it can be seen that the behaviour of the corrections strongly depends on the choice of $m_{\tilde{g}}$. The figure shows M_h as a function of $m_{\tilde{g}}$ for $\mu = -1000\,\text{GeV}$, $\tan\beta = 50$ and $M_A = 700\,\text{GeV}$. For $m_{\tilde{g}} \lesssim 1000\,\text{GeV}$ all schemes lead to an increase of M_h from the subleading $\mathcal{O}(\alpha_b\alpha_s)$ corrections. For $m_{\tilde{g}} \gtrsim 1500\,\text{GeV}$, on the other hand, all schemes lead to a decrease, where the size of the individual corrections also strongly varies with $m_{\tilde{g}}$. Accordingly, the relative size of the corrections in the different schemes also varies with $m_{\tilde{g}}$. Corrections up to about 3 GeV are possible. The differences between the three schemes are of $\mathcal{O}(2\,\text{GeV})$ for large $m_{\tilde{g}}$. It should be noted that the effects of the higher-order corrections to M_h do not decouple with large $m_{\tilde{g}}$. The corrections at $\mathcal{O}(\alpha_t\alpha_s)$ [19] as well as $\mathcal{O}(\alpha_b\alpha_s)$ grow logarithmically in the renormalisation schemes that we have adopted.

The above analysis of the three schemes "$m_b\ \overline{\rm DR}$", "A_b, $\theta_{\tilde{b}}\ \overline{\rm DR}$", and "$A_b$, $\theta_{\tilde{b}}$ OS" in various parameter regions yields numerically well-behaved and physically meaningful results. As there is no clear preference for one of the schemes on physical grounds, the difference between the results obtained in the three schemes can be interpreted as an indication of the possible size of missing higher-order corrections. The size of the individual corrections and also the differences between the renormalisation schemes sensitively depend on the input parameters. Typically we find that the genuine two-loop corrections in the $b/\tilde{b}$ sector yield a shift in M_h of $\mathcal{O}(1\,\text{GeV})$. The differences between the three schemes are usually somewhat smaller.

4.3 Numerical analysis of the renormalisation scale dependence

While in the previous section we compared the results of different renormalisation scheme, we now focus on the "$m_b\ \overline{\rm DR}$" scheme and investigate the effect of varying the renormalisation scale of the $\mathcal{O}(\alpha_b\alpha_s)$ result obtained in this scheme. We vary the scale within the interval $m_t/2 \leq \mu^{\overline{\rm DR}} \leq 2\,m_t$, resulting in a shift which is formally of $\mathcal{O}(\alpha_b\alpha_s^2)$. The results are shown as a function of $m_{\tilde{g}}$ for $\tan\beta = 50$ in Fig. 12 for $M_A = 120\,\text{GeV}$ and $M_A = 700\,\text{GeV}$.

The $\mu^{\overline{\rm DR}}$ variation of the leading contribution (the $\mathcal{O}(\alpha_t\alpha_s)$ result including resummation) is shown as the dark shaded (black) band. The results including the subleading corrections in the "$m_b\ \overline{\rm DR}$" scheme are shown as a light shaded (red) band. It can be seen that the variation with $\mu^{\overline{\rm DR}}$ is strongly reduced by the inclusion of the subleading contributions. The variation with $\mu^{\overline{\rm DR}}$ within the "$m_b\ \overline{\rm DR}$" scheme is tiny for $m_{\tilde{g}} \lesssim 500\,\text{GeV}$, and reaches $\pm 2\,\text{GeV}$ for large $m_{\tilde{g}}$ values. Thus, the $\mu^{\overline{\rm DR}}$ variation causes a similar shift in M_h as the comparison between the three renormalisation schemes discussed above.

We have also analysed the variation with $\mu^{\overline{\rm DR}}$ in the case $\mu > 0$, which is not shown here. As for negative μ, the variation with $\mu^{\overline{\rm DR}}$ is of the same order as the differences between the three renormalisation schemes; see Fig. 8. Therefore, for $\mu > 0$ the unknown higher-order corrections to M_h from the $b/\tilde{b}$ sector can be estimated to be of $\mathcal{O}(100\,\text{MeV})$.

4.4 Comparison with existing calculations

Finally we compare our result with the existing calculation of the $\mathcal{O}(\alpha_b\alpha_s)$ corrections presented in [26]. The renormalisation employed there consists of an on-shell renormalisation of the two scalar bottom masses and the on-shell condition for A_b shown in Sect. 3.2.4. We denote it as "$m_{\tilde{b}}$, A_b OS" renormalisation. Thus, the differences between our "A_b, $\theta_{\tilde{b}}$ OS" and the "$m_{\tilde{b}}$, A_b OS" renormalisation are the different treatment of the $m_{\tilde{b}_1}$ renormalisation, as well as the treatment of $\tan\beta$. We kept $\tan\beta$

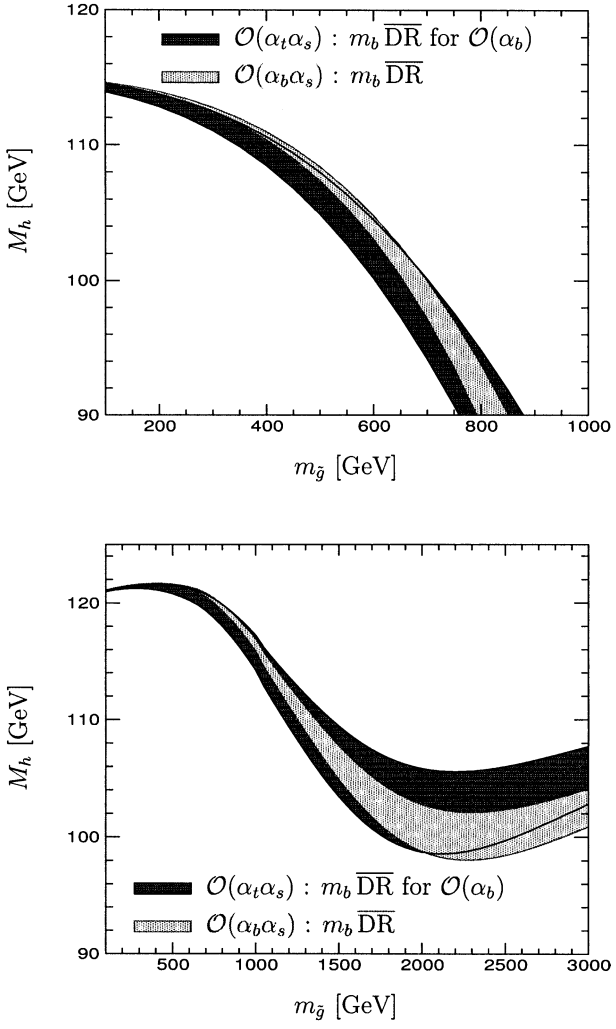

Fig. 12. $\mu^{\overline{\rm DR}}$ dependence of M_h as a function of $m_{\tilde g}$ for $M_A = 120\,\text{GeV}$ (upper plot) and $M_A = 700\,\text{GeV}$ (lower plot) for $\mu = -1000\,\text{GeV}$, $\tan\beta = 50$. The black area corresponds to the $\mathcal{O}(\alpha_t\alpha_s)$ result including resummation, i.e. the result without the subleading two-loop $\mathcal{O}(\alpha_b\alpha_s)$ terms

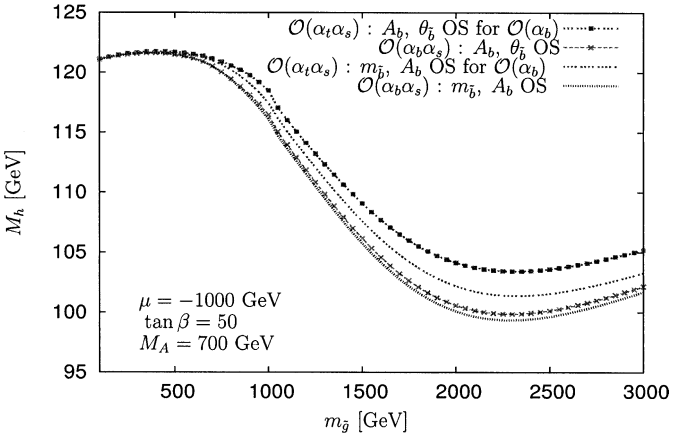

Fig. 13. Comparison of our $\mathcal{O}(\alpha_b\alpha_s)$ result for M_h in the "A_b, $\theta_{\tilde b}$ OS" scheme and the result of [26] ("$m_{\tilde b}$, A_b OS" scheme) as a function of $m_{\tilde g}$. The $\mathcal{O}(\alpha_t\alpha_s)$ results in the two schemes, where the subleading $\mathcal{O}(\alpha_b\alpha_s)$ corrections are omitted (using the appropriate renormalised parameters), are also shown

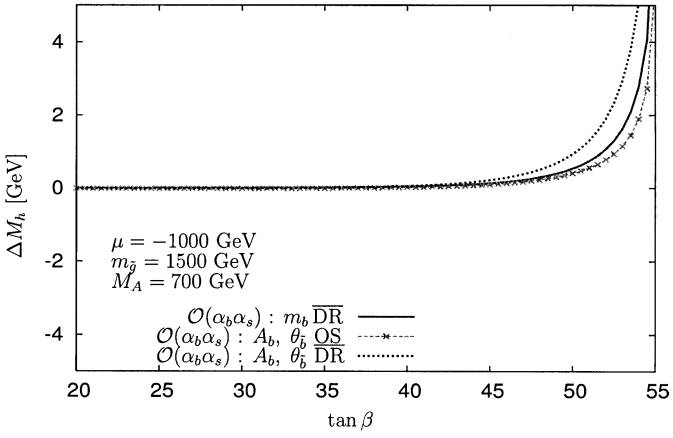

Fig. 14. Comparison of our $\mathcal{O}(\alpha_b\alpha_s)$ result in three different renormalisation schemes and the result of [26]. The three curves for ΔM_h show the difference between our result in each of the three schemes and the result of [26] as a function of $\tan\beta$

as a free parameter, whereas in [26] it was set to infinity in the subleading $\mathcal{O}(\alpha_b\alpha_s)$ corrections. In [26] the shift of the sbottom masses due to the SU(2)-invariance was taken into account in the numerical evaluation of the sbottom masses following the prescription in [56] (see also [42]).

Our result for M_h in the "A_b, $\theta_{\tilde b}$ OS" scheme is compared with the result of [26] in Fig. 13. For the implementation of the latter ("$m_{\tilde b}$, A_b OS" scheme) the Fortran code of [26] for the numerical evaluation of the $\mathcal{O}(\alpha_s\alpha_b)$ corrections to the Higgs-boson self-energies has been used [57]. Thereby the input values were determined according to (51) and (52). Using these input values for A_b and m_b the sbottom masses were calculated taking the sbottom mass shift into account [56]. M_h is shown as function of $m_{\tilde g}$ for $\mu < 0$, $\tan\beta = 50$, and $M_A = 700\,\text{GeV}$. Our result in the "A_b, $\theta_{\tilde b}$ OS" scheme is shown as the dash-star (green) curve, while the result of [26] ("$m_{\tilde b}$, A_b OS" scheme) is given by the fine-dotted (pink) curve. The leading contribution in the two schemes, i.e. the $\mathcal{O}(\alpha_t\alpha_s)$ result including resummation, is also shown: the light-dot-dashed (orange) curve shows the $\mathcal{O}(\alpha_t\alpha_s)$ result using the "A_b, $\theta_{\tilde b}$ OS" renormalised parameters; the corresponding result for the "$m_{\tilde b}$, A_b OS" renormalised parameters is shown as the light-dotted (gray) curve.

Figure 13 shows that the $\mathcal{O}(\alpha_t\alpha_s)$ results in the two schemes differ from each other by up to 2 GeV for large $m_{\tilde g}$. The inclusion of the subleading two-loop corrections reduces this difference significantly. Our result in the "A_b, $\theta_{\tilde b}$ OS" scheme agrees with the result of [26] to better than 0.5 GeV.

In Fig. 14 we compare our result in each of the three schemes discussed above, i.e. the "A_b, $\theta_{\tilde b}$ OS", the "m_b $\overline{\rm DR}$" and the "A_b, $\theta_{\tilde b}$ $\overline{\rm DR}$" schemes, with the result of [26]. The difference ΔM_h between our result and the result of [26] is shown for each of the three schemes as a function of $\tan\beta$ for $m_{\tilde g} = 1500\,\text{GeV}$, $\mu = -1000\,\text{GeV}$, and $M_A = 700\,\text{GeV}$. The differences stay below 1 GeV for $\tan\beta \lesssim 50$, where our result in the "A_b, $\theta_{\tilde b}$ $\overline{\rm DR}$" scheme shows the

biggest deviation from the result of [26], while as expected, the difference is smallest for the "A_b, $\theta_{\tilde{b}}$ OS" scheme. For $\tan\beta > 50$ large deviations occur because of the sharp decrease of M_h in this region (see e.g. Fig. 7).

5 Conclusions

We have obtained results for the two-loop $\mathcal{O}(\alpha_b\alpha_s)$ corrections to the neutral $\mathcal{CP}$-even Higgs-boson masses in the MSSM within different renormalisation schemes. The leading $\tan\beta$-enhanced contributions of the $b/\tilde{b}$ sector can be incorporated into an appropriately chosen bottom Yukawa coupling, for which we use the bottom-quark mass in the $\overline{\rm DR}$ scheme with a resummation of the leading contributions. We have analysed in detail the impact of the genuine (subleading) $\mathcal{O}(\alpha_b\alpha_s)$ two-loop corrections in different parts of the MSSM parameter space and we have compared the results obtained in the different schemes.

We have shown that an on-shell scheme that is frequently used in the $t/\tilde{t}$ sector leads to numerically unstable results if it is applied in the $b/\tilde{b}$ sector. The origin of the huge corrections in this scheme was traced to the fact that it involves a renormalisation condition for the sbottom mixing angle, $\theta_{\tilde{b}}$, rather than for the trilinear coupling, A_b.

The other three schemes that we have analysed yield numerically well-behaved and physically meaningful results. For $\mu > 0$ the effect of the genuine $\mathcal{O}(\alpha_b\alpha_s)$ two-loop corrections is rather small, typically of $\mathcal{O}(100\,\text{MeV})$. Corrections at this level will nevertheless be relevant in view of the prospective accuracy of measurements in the Higgs sector and of the top-quark mass at the ILC. For $\mu < 0$ the effective bottom Yukawa coupling increases, leading to an enhancement of the effects from the $b/\tilde{b}$ sector. While the constraints arising from the measurement of the anomalous magnetic moment of the muon favour the positive sign of μ, it seems premature at the present stage to discard the parameter region with $\mu < 0$. For large values of $\tan\beta$ and $m_{\tilde{g}}$ and large negative values of μ we find that the genuine $\mathcal{O}(\alpha_b\alpha_s)$ corrections can amount up to 3 GeV. We have compared our result for the $\mathcal{O}(\alpha_b\alpha_s)$ corrections with the existing result in the literature, which was obtained in the limit of $\tan\beta \to \infty$, and found good agreement.

The comparison of the results in the different schemes that we have analysed and the investigation of the renormalisation scale dependence give an indication of the possible size of missing higher-order corrections in the $b/\tilde{b}$ sector. For $\mu > 0$ the higher-order corrections from the $b/\tilde{b}$ sector (beyond $\mathcal{O}(\alpha_b\alpha_s)$) appear to be sufficiently well under control even in view of the prospective ILC accuracy. This applies especially to the "m_b $\overline{\rm DR}$" scheme, where the corrections beyond the improved one-loop result have been found to be particularly small. For $\mu < 0$, on the other hand, sizable higher-order corrections from the $b/\tilde{b}$ sector are possible. The size of the individual corrections and also the difference between the analysed schemes varies significantly with the relevant parameters, μ, $\tan\beta$, $m_{\tilde{g}}$ and M_A. We estimate the uncertainty from missing higher-order corrections in the $b/\tilde{b}$ sector to be about 2 GeV in this region of parameter space.

The results obtained will be implemented into the Fortran code FeynHiggs [58,59]. The evaluation of the results within the three schemes will allow one to obtain an estimate of the size of the missing higher-order corrections as a function of the chosen input parameters.

Acknowledgements. We thank A. Hoang, U. Nierste, P. Slavich and D. Stöckinger for helpful discussions. We are grateful to P. Slavich for providing the Fortran code for the "$m_{\tilde{b}}$, A_b OS" renormalisation scheme. S.H. and G.W. thank the Max Planck Institut für Physik, München, for kind hospitality during part of this work. G.W. thanks the CERN theory group for kind hospitality during the final stage of this paper. This work has been supported by the European Community's Human Potential Programme under contract HPRN-CT-2000-00149 "Physics at Colliders".

Appendix: Counterterms of the quark/squark sector

In Sect. 3 the counterterms have been given using the definitions (14) and (16) for the sfermion masses and mixing angles. In this appendix the counterterms are given in a more general way allowing one to use also other definitions for the sfermion masses and mixing angles. Introducing a counterterm for the mixing angle needs a certain choice of definitions of the sfermion masses and mixing angles. Instead of using an explicit mixing angle counterterm the counterterm $\delta Y_{\tilde{q}}$ is introduced as

$$\delta Y_{\tilde{q}} = (\mathcal{U}_{\tilde{q}}\delta\mathcal{M}_{\tilde{q}}\mathcal{U}_{\tilde{q}}^{\dagger})_{12} = (\mathcal{U}_{\tilde{q}}\delta\mathcal{M}_{\tilde{q}}\mathcal{U}_{\tilde{q}}^{\dagger})_{21}\,, \tag{54}$$

where the counterterm mass matrix $\delta\mathcal{M}_{\tilde{q}}$ contains the counterterms of the parameters appearing in (13). With the definitions (14) and (16) $\delta Y_{\tilde{q}}$ is related to the mixing angle counterterm as follows:

$$\delta Y_{\tilde{q}} = (m^2_{\tilde{q}_1} - m^2_{\tilde{q}_2})\,\delta\theta_{\tilde{q}}\,. \tag{55}$$

Top quark/squark sector

The counterterms for the top-quark mass (18) and the stop masses (20) are already in a general form. The counterterm for the mixing angle (21) is replaced by

$$\delta Y_{\tilde{t}} = \frac{1}{2}\left(\text{Re}\,\Sigma_{\tilde{t}_{12}}(m^2_{\tilde{t}_1}) + \text{Re}\,\Sigma_{\tilde{t}_{12}}(m^2_{\tilde{t}_2})\right), \tag{56}$$

and the counterterm of the A parameter (23) is rewritten as

$$\begin{aligned}\delta A_t = \frac{1}{m_t}\Big[&U_{\tilde{t}_{11}}U_{\tilde{t}_{12}}\left(\delta m^2_{\tilde{t}_1} - \delta m^2_{\tilde{t}_2}\right) \\ &+(U_{\tilde{t}_{11}}U_{\tilde{t}_{22}} + U_{\tilde{t}_{12}}U_{\tilde{t}_{21}})\,\delta Y_{\tilde{t}} - \delta m_t\,(A_t - \mu\cot\beta)\Big]\,.\end{aligned} \tag{57}$$

Analogous to the top-quark/squark sector

As in the top-quark/squark sector the counterterm for the mixing angle (30) is replaced by

$$\delta Y_{\tilde{b}} = \frac{1}{2}\left(\mathrm{Re}\,\Sigma_{\tilde{b}_{12}}(m^2_{\tilde{b}_1}) + \mathrm{Re}\,\Sigma_{\tilde{b}_{12}}(m^2_{\tilde{b}_2})\right). \quad (58)$$

The dependent counterterms of the $\tilde{b}_1$-mass (26) and of the A parameter (31) are rewritten as follows:

$$\begin{aligned}
&\delta m^2_{\tilde{b}_1} \\
&= \frac{1}{U^2_{\tilde{b}_{11}}}\Big[-U^2_{\tilde{b}_{12}}\delta m^2_{\tilde{b}_2} + 2U_{\tilde{b}_{12}}U_{\tilde{b}_{22}}\delta Y_{\tilde{b}} + U^2_{\tilde{t}_{11}}\delta m^2_{\tilde{t}_1} \quad (59)\\
&\quad + U^2_{\tilde{t}_{12}}\delta m^2_{\tilde{t}_2} - 2U_{\tilde{t}_{12}}U_{\tilde{t}_{22}}\delta Y_{\tilde{t}} + (2m_b\delta m_b - 2m_t\delta m_t)\Big],\\
\delta A_b &= \frac{1}{m_b}\left[-\frac{U_{\tilde{b}_{12}}}{U_{\tilde{b}_{11}}}\delta m^2_{\tilde{b}_2} + \frac{U_{\tilde{b}_{22}}}{U_{\tilde{b}_{11}}}\delta Y_{\tilde{b}}\right.\\
&\quad -\delta m_b\left(A_b - \mu\tan\beta - 2\frac{U_{\tilde{b}_{12}}}{U_{\tilde{b}_{11}}}m_b\right) \quad (60)\\
&\quad + \frac{U_{\tilde{b}_{12}}}{U_{\tilde{b}_{11}}}\left(U^2_{\tilde{t}_{11}}\delta m^2_{\tilde{t}_1} + U^2_{\tilde{t}_{12}}\delta m^2_{\tilde{t}_2} - 2U_{\tilde{t}_{12}}U_{\tilde{t}_{22}}\delta Y_{\tilde{t}}\right.\\
&\quad \left.\left. -2m_t\delta m_t\right)\right].
\end{aligned}$$

$\overline{\mathrm{DR}}$ bottom-quark mass

The A parameter counterterm (34) is written in the following way:

$$\begin{aligned}
\delta A_b &= \frac{1}{m_b}\left[-\frac{U_{\tilde{b}_{12}}}{U_{\tilde{b}_{11}}}\,\mathrm{Re}\,\Sigma^{\mathrm{div}}_{\tilde{b}_{22}}(m^2_{\tilde{b}_2})\right.\\
&\quad + \frac{U_{\tilde{b}_{22}}}{2U_{\tilde{b}_{11}}}\left(\mathrm{Re}\,\Sigma^{\mathrm{div}}_{\tilde{b}_{12}}(m^2_{\tilde{b}_1}) + \mathrm{Re}\,\Sigma^{\mathrm{div}}_{\tilde{b}_{12}}(m^2_{\tilde{b}_2})\right)\\
&\quad + \frac{U_{\tilde{b}_{12}}}{U_{\tilde{b}_{11}}}\left(U^2_{\tilde{t}_{11}}\,\mathrm{Re}\,\Sigma^{\mathrm{div}}_{\tilde{t}_{11}}(m^2_{\tilde{t}_1}) + U^2_{\tilde{t}_{12}}\,\mathrm{Re}\,\Sigma^{\mathrm{div}}_{\tilde{t}_{22}}(m^2_{\tilde{t}_2})\right.\\
&\quad - U_{\tilde{t}_{12}}U_{\tilde{t}_{22}}\left(\mathrm{Re}\,\Sigma^{\mathrm{div}}_{\tilde{t}_{12}}(m^2_{\tilde{t}_1}) + \mathrm{Re}\,\Sigma^{\mathrm{div}}_{\tilde{t}_{12}}(m^2_{\tilde{t}_2})\right)\\
&\quad \left.\left. - m^2_t\left(\mathrm{Re}\,\Sigma^{\mathrm{div}}_{t_{\mathrm{L}}}(m^2_t) + \mathrm{Re}\,\Sigma^{\mathrm{div}}_{t_{\mathrm{R}}}(m^2_t) + 2\,\mathrm{Re}\,\Sigma^{\mathrm{div}}_{t_S}(m^2_t)\right)\right)\right]\\
&\quad + \frac{1}{2}\left(2\frac{U_{\tilde{b}_{12}}}{U_{\tilde{b}_{11}}}m_b - A_b + \mu\tan\beta\right) \quad (61)\\
&\quad \times\left(\mathrm{Re}\,\Sigma^{\mathrm{div}}_{b_{\mathrm{L}}}(m^2_b) + \mathrm{Re}\,\Sigma^{\mathrm{div}}_{b_{\mathrm{R}}}(m^2_b) + 2\,\mathrm{Re}\,\Sigma^{\mathrm{div}}_{b_S}(m^2_b)\right),
\end{aligned}$$

avoiding an explicit definition of the mixing angles. The dependent counterterm for the mixing angle (35) is replaced by

$$\begin{aligned}
&\delta Y_{\tilde{b}} \\
&= \frac{U_{\tilde{b}_{11}}}{U_{\tilde{b}_{22}}}m_b\delta A_b + \frac{U_{\tilde{b}_{11}}}{U_{\tilde{b}_{22}}}\delta m_b\left(A_b - \mu\tan\beta - 2\frac{U_{\tilde{b}_{12}}}{U_{\tilde{b}_{11}}}m_b\right)\\
&\quad + \frac{U_{\tilde{b}_{12}}}{U_{\tilde{b}_{22}}}\left[\delta m^2_{\tilde{b}_2} - U^2_{\tilde{t}_{11}}\delta m^2_{\tilde{t}_1} - U^2_{\tilde{t}_{12}}\delta m^2_{\tilde{t}_2} + 2U_{\tilde{t}_{12}}U_{\tilde{t}_{22}}\delta Y_{\tilde{t}}\right.\\
&\quad \left. + 2m_t\delta m_t\right], \quad (62)
\end{aligned}$$

and the counterterm for the $\tilde{b}_1$-mass (36) by

$$\begin{aligned}
\delta m^2_{\tilde{b}_1} &= \frac{1}{U^2_{\tilde{b}_{11}}}\left[(1 - 2U^2_{\tilde{b}_{12}})\right.\\
&\quad \times\left(U^2_{\tilde{t}_{11}}\delta m^2_{\tilde{t}_1} + U^2_{\tilde{t}_{12}}\delta m^2_{\tilde{t}_2} - 2U_{\tilde{t}_{12}}U_{\tilde{t}_{22}}\delta Y_{\tilde{t}} - 2m_t\delta m_t\right)\\
&\quad + U^2_{\tilde{b}_{12}}\delta m^2_{\tilde{b}_2} + 2U_{\tilde{b}_{11}}U_{\tilde{b}_{12}}m_b\delta A_b\\
&\quad + \left(2U_{\tilde{b}_{12}}U_{\tilde{b}_{11}}(A_b - \mu\tan\beta)\right.\\
&\quad \left.\left. + 2(1 - 2U^2_{\tilde{b}_{12}})m_b\right)\delta m_b\right]. \quad (63)
\end{aligned}$$

$\overline{\mathrm{DR}}$ mixing angle and A_b

The counterterm for the mixing angle (40) is replaced by

$$\delta Y_{\tilde{b}} = \frac{1}{2}\left(\mathrm{Re}\,\Sigma^{\mathrm{div}}_{\tilde{b}_{12}}(m^2_{\tilde{b}_1}) + \mathrm{Re}\,\Sigma^{\mathrm{div}}_{\tilde{b}_{12}}(m^2_{\tilde{b}_2})\right). \quad (64)$$

The dependent counterterm for the bottom-quark mass (41) is rewritten as the following combination of counterterms:

$$\begin{aligned}
\delta m_b &= -\left[m_b\,\delta A_b - \frac{U_{\tilde{b}_{22}}}{U_{\tilde{b}_{11}}}\delta Y_{\tilde{b}} + \frac{U_{\tilde{b}_{12}}}{U_{\tilde{b}_{11}}}\delta m^2_{\tilde{b}_2}\right.\\
&\quad - \frac{U_{\tilde{b}_{12}}}{U_{\tilde{b}_{11}}}\left(U^2_{\tilde{t}_{11}}\delta m^2_{\tilde{t}_1} + U^2_{\tilde{t}_{12}}\delta m^2_{\tilde{t}_2} - 2U_{\tilde{t}_{12}}U_{\tilde{t}_{22}}\delta Y_{\tilde{t}}\right.\\
&\quad \left.\left. -2m_t\,\delta m_t\right)\right]\\
&\quad \times\left[A_b - \mu\tan\beta - 2m_b\frac{U_{\tilde{b}_{12}}}{U_{\tilde{b}_{11}}}\right]^{-1}. \quad (65)
\end{aligned}$$

The counterterm for the $\tilde{b}_1$-mass is obtained by inserting the expression (65) for the bottom-quark mass into the expression (59).

On-shell mixing angle and A_b

The renormalised vertex (44) has the following general form:

$$\begin{aligned}
\hat{\Lambda}(p^2_A, p^2_{\tilde{b}_1}, p^2_{\tilde{b}_2}) &= \Lambda(p^2_A, p^2_{\tilde{b}_1}, p^2_{\tilde{b}_2})\\
&\quad + \frac{\mathrm{i}e}{2M_W\sin\theta_{\mathrm{W}}}(U_{\tilde{b}_{11}}U_{\tilde{b}_{22}} - U_{\tilde{b}_{12}}U_{\tilde{b}_{21}})\\
&\quad \times\left[m_b\tan\beta\delta A_b + (\mu + \tan\beta A_b)\right.\\
&\quad \left.\times\left(\delta m_b + \frac{1}{2}m_b(\delta Z_{\tilde{b}_1\tilde{b}_1} + \delta Z_{\tilde{b}_2\tilde{b}_2})\right)\right]. \quad (66)
\end{aligned}$$

Using the renormalisation condition (43) the counterterms of the A parameter and the bottom-quark mass can be derived as

$$
\begin{aligned}
\delta A_b = {} & \mathrm{i}\frac{M_W \sin\theta_W}{e\, m_b \tan\beta (U_{\tilde{b}_{11}} U_{\tilde{b}_{22}} - U_{\tilde{b}_{12}} U_{\tilde{b}_{21}})} \\
& \times \Big(\Lambda(0, m^2_{\tilde{b}_1}, m^2_{\tilde{b}_1}) + \Lambda(0, m^2_{\tilde{b}_2}, m^2_{\tilde{b}_2}) \Big) \\
& - \frac{\mu + A_b \tan\beta}{2\tan\beta} (\delta Z_{\tilde{b}_1\tilde{b}_1} + \delta Z_{\tilde{b}_2\tilde{b}_2}) \\
& - \frac{\mu + A_b \tan\beta}{m_b \tan\beta} \left[\mathrm{i}\frac{M_W \sin\theta_W}{e \tan\beta (U_{\tilde{b}_{11}} U_{\tilde{b}_{22}} - U_{\tilde{b}_{12}} U_{\tilde{b}_{21}})} \right. \\
& \times \Big(\Lambda(0, m^2_{\tilde{b}_1}, m^2_{\tilde{b}_1}) + \Lambda(0, m^2_{\tilde{b}_2}, m^2_{\tilde{b}_2}) \Big) \\
& - \frac{m_b(\mu + A_b \tan\beta)}{2\tan\beta} (\delta Z_{\tilde{b}_1\tilde{b}_1} + \delta Z_{\tilde{b}_2\tilde{b}_2}) \\
& + \frac{U_{\tilde{b}_{12}}}{U_{\tilde{b}_{11}}} \delta m^2_{\tilde{b}_2} - \frac{U_{\tilde{b}_{22}}}{U_{\tilde{b}_{11}}} \delta Y_{\tilde{b}} \\
& - \frac{U_{\tilde{b}_{12}}}{U_{\tilde{b}_{11}}} \Big(U^2_{\tilde{t}_{11}} \delta m^2_{\tilde{t}_1} + U^2_{\tilde{t}_{12}} \delta m^2_{\tilde{t}_2} - 2 U_{\tilde{t}_{12}} U_{\tilde{t}_{22}} \delta Y_{\tilde{t}} \\
& \left. - 2 m_t \delta m_t \Big) \right] \\
& \times \left[\mu \left(\tan\beta + \frac{1}{\tan\beta} \right) + 2 m_b \frac{U_{\tilde{b}_{12}}}{U_{\tilde{b}_{11}}} \right]^{-1} , \qquad (67)
\end{aligned}
$$

and

$$
\begin{aligned}
\delta m_b = {} & \left[\mathrm{i}\frac{M_W \sin\theta_W}{e\, \tan\beta (U_{\tilde{b}_{11}} U_{\tilde{b}_{22}} - U_{\tilde{b}_{12}} U_{\tilde{b}_{21}})} \right. \\
& \times \Big(\Lambda(0, m^2_{\tilde{b}_1}, m^2_{\tilde{b}_1}) + \Lambda(0, m^2_{\tilde{b}_2}, m^2_{\tilde{b}_2}) \Big) \\
& - \frac{m_b(\mu + A_b \tan\beta)}{2\tan\beta} (\delta Z_{\tilde{b}_1\tilde{b}_1} + \delta Z_{\tilde{b}_2\tilde{b}_2}) \\
& - \frac{U_{\tilde{b}_{22}}}{U_{\tilde{b}_{11}}} \delta Y_{\tilde{b}} + \frac{U_{\tilde{b}_{12}}}{U_{\tilde{b}_{11}}} \delta m^2_{\tilde{b}_2} \\
& - \frac{U_{\tilde{b}_{12}}}{U_{\tilde{b}_{11}}} \Big(U^2_{\tilde{t}_{11}} \delta m^2_{\tilde{t}_1} + U^2_{\tilde{t}_{12}} \delta m^2_{\tilde{t}_2} - 2 U_{\tilde{t}_{12}} U_{\tilde{t}_{22}} \delta Y_{\tilde{t}} \\
& \left. - 2 m_t \delta m_t \Big) \right] \\
& \times \left[\mu \left(\tan\beta + \frac{1}{\tan\beta} \right) + 2 m_b \frac{U_{\tilde{b}_{12}}}{U_{\tilde{b}_{11}}} \right]^{-1} , \qquad (68)
\end{aligned}
$$

replacing (45) and (47). The counterterm of the mixing angle (42) is replaced by (58).

References

1. H.P. Nilles, Phys. Rep. **110**, 1 (1984); H.E. Haber, G.L. Kane, Phys. Rep. **117**, 75 (1985); R. Barbieri, Riv. Nuovo Cim. **11**, 1 (1988)
2. LEP Higgs working group, Phys. Lett. B **565**, 61 (2003), hep-ex/0306033
3. LEP Higgs working group, hep-ex/0107030; hep-ex/0107031; LHWG-Note 2004-01, see lep-higgs.web.cern.ch/LEPHIGGS/papers/
4. ATLAS Collaboration, Detector and Physics Performance Technical Design Report, CERN/LHCC/99-15 (1999), see atlasinfo.cern.ch/Atlas/GROUPS/PHYSICS/TDR/access.html; CMS Collaboration, see cmsinfo.cern.ch/Welcome.html/CMSdocuments/CMSplots/
5. D. Zeppenfeld, R. Kinnunen, A. Nikitenko, E. Richter-Was, Phys. Rev. D **62**, 013009 (2000), hep-ph/0002036; A. Belyaev, L. Reina, JHEP **0208**, 041 (2002), hep-ph/0205270; M. Dührssen, ATL-PHYS-2003-030, available from cdsweb.cern.ch
6. M. Dührssen, S. Heinemeyer, H. Logan, D. Rainwater, G. Weiglein, D. Zeppenfeld, hep-ph/0406323
7. J. Aguilar-Saavedra et al., TESLA TDR Part 3: Physics at an e^+e^- Linear Collider, hep-ph/0106315, see tesla.desy.de/tdr/
8. T. Abe et al. [American Linear Collider Working Group Collaboration], Resource book for Snowmass 2001, hep-ex/0106056
9. K. Abe et al. [ACFA Linear Collider Working Group Collaboration], hep-ph/0109166
10. J. Ellis, G. Ridolfi, F. Zwirner, Phys. Lett. B **257**, 83 (1991); Y. Okada, M. Yamaguchi, T. Yanagida, Prog. Theor. Phys. **85**, 1 (1991); H. Haber, R. Hempfling, Phys. Rev. Lett. **66**, 1815 (1991)
11. A. Brignole, Phys. Lett. B **281**, 284 (1992)
12. P. Chankowski, S. Pokorski, J. Rosiek, Phys. Lett. B **286**, 307 (1992); Nucl. Phys. B **423**, 423 (1994), hep-ph/9303309
13. A. Dabelstein, Nucl. Phys. B **456**, 25 (1995), hep-ph/9503443; Z. Phys. C **67**, 495 (1995), hep-ph/9409375
14. R. Hempfling, A. Hoang, Phys. Lett. B **331**, 99 (1994), hep-ph/9401219
15. A. Hoang, Applications of Two-Loop Calculations in the Standard Model and its Minimal Supersymmetric Extension, PhD thesis, Universität Karlsruhe, Shaker Verlag, Aachen 1995
16. M. Carena, J. Espinosa, M. Quirós, C. Wagner, Phys. Lett. B **355**, 209 (1995), hep-ph/9504316; M. Carena, M. Quirós, C. Wagner, Nucl. Phys. B **461**, 407 (1996), hep-ph/9508343
17. H. Haber, R. Hempfling, A. Hoang, Z. Phys. C **75**, 539 (1997), hep-ph/9609331
18. S. Heinemeyer, W. Hollik, G. Weiglein, Phys. Rev. D **58**, 091701 (1998), hep-ph/9803277; Phys. Lett. B **440**, 296 (1998), hep-ph/9807423
19. S. Heinemeyer, W. Hollik, G. Weiglein, Eur. Phys. J. C **9**, 343 (1999), hep-ph/9812472
20. R. Zhang, Phys. Lett. B **447**, 89 (1999), hep-ph/9808299; J. Espinosa, R. Zhang, JHEP **0003**, 026 (2000), hep-ph/9912236
21. G. Degrassi, P. Slavich, F. Zwirner, Nucl. Phys. B **611**, 403 (2001), hep-ph/0105096
22. M. Carena, H. Haber, S. Heinemeyer, W. Hollik, C. Wagner, G. Weiglein, Nucl. Phys. B **580**, 29 (2000), hep-ph/0001002

23. S. Heinemeyer, W. Hollik, G. Weiglein, hep-ph/9910283; J. Espinosa, R. Zhang, JHEP **0003**, 026 (2000), hep-ph/9912236
24. J. Espinosa, R. Zhang, Nucl. Phys. B **586**, 3 (2000), hep-ph/0003246
25. A. Brignole, G. Degrassi, P. Slavich, F. Zwirner, Nucl. Phys. B **631**, 195 (2002), hep-ph/0112177
26. A. Brignole, G. Degrassi, P. Slavich, F. Zwirner, Nucl. Phys. B **643**, 79 (2002), hep-ph/0206101
27. G. Degrassi, A. Dedes, P. Slavich, Nucl. Phys. B **672**, 144 (2003), hep-ph/0305127
28. S. Martin, Phys. Rev. D **65**, 116003 (2002), hep-ph/0111209; D **66**, 096001 (2002), hep-ph/0206136; D **67**, 095012 (2003), hep-ph/0211366; D **68**, 075002 (2003), hep-ph/0307101; D **70**, 016005 (2004), hep-ph/0312092
29. S. Martin, hep-ph/0405022
30. T. Banks, Nucl. Phys. B **303**, 172 (1988); L. Hall, R. Rattazzi, U. Sarid, Phys. Rev. D **50**, 7048 (1994), hep-ph/9306309; R. Hempfling, Phys. Rev. D **49**, 6168 (1994); M. Carena, M. Olechowski, S. Pokorski, C. Wagner, Nucl. Phys. B **426**, 269 (1994), hep-ph/9402253
31. M. Carena, D. Garcia, U. Nierste, C. Wagner, Nucl. Phys. B **577**, 577 (2000), hep-ph/9912516; H. Eberl, K. Hidaka, S. Kraml, W. Majerotto, Y. Yamada, Phys. Rev. D **62**, 055006 (2000), hep-ph/9912463
32. G. Degrassi, S. Heinemeyer, W. Hollik, P. Slavich, G. Weiglein, Eur. Phys. J. C **28**, 133 (2003), hep-ph/0212020
33. S. Heinemeyer, hep-ph/0407244
34. B. Allanach, A. Djouadi, J. Kneur, W. Porod, P. Slavich, JHEP **0409**, 044 (2004), hep-ph/0406166
35. J. Gunion, H. Haber, G. Kane, S. Dawson, The Higgs hunter's guide (Addison-Wesley, 1990)
36. J. Küblbeck, M. Böhm, A. Denner, Comp. Phys. Comm. **60**, 165 (1990); T. Hahn, Comput. Phys. Comm. **140**, 418 (2001), hep-ph/0012260.
The program is available via www.feynarts.de
37. T. Hahn, C. Schappacher, Comput. Phys. Comm. **143**, 54 (2002), hep-ph/0105349
38. G. Weiglein, R. Scharf, M. Böhm, Nucl. Phys. B **416**, 606 (1994), hep-ph/9310358; G. Weiglein, R. Mertig, R. Scharf, M. Böhm, in New Computing Techniques in Physics Research 2, edited by D. Perret-Gallix (World Scientific, Singapore 1992), p. 617
39. G. 't Hooft, M. Veltman, Nucl. Phys. B **153**, 365 (1979)
40. A. Davydychev, J. Tausk, Nucl. Phys. B **397**, 123 (1993); F. Berends, J. Tausk, Nucl. Phys. B **421**, 456 (1994)
41. W. Hollik, H. Rzehak, Eur. Phys. J. C **32**, 127 (2003), hep-ph/0305328
42. A. Djouadi, P. Gambino, S. Heinemeyer, W. Hollik, C. Jünger, G. Weiglein, Phys. Rev. Lett. **78**, 3626 (1997), hep-ph/9612363; Phys. Rev. D **57**, 4179 (1998), hep-ph/9710438
43. S. Eidelman et al., Phys. Lett. B **592**, 1 (2004)
44. W. Siegel, Phys. Lett. B **84**, 193 (1979); D. Capper, D. Jones, P. van Nieuwenhuizen, Nucl. Phys. B **167**, 479 (1980)
45. A. El-Khadra, M. Luke, Ann. Rev. Nucl. Part. Sci. **52**, 201 (2002), hep-ph/0208114
46. J. Guasch, P. Häfliger, M. Spira, Phys. Rev. D **68**, 115001 (2003), hep-ph/0305101
47. T. Moroi, Phys. Rev. D **53**, 6565 (1996) [Erratum D **56**, 4424 (1997)], hep-ph/9512396
48. A. Czarnecki, W. Marciano, Phys. Rev. D **64**, 013014 (2001), hep-ph/0102122
49. [The Muon g-2 Collaboration], Phys. Rev. Lett. **92**, 161802 (2004), hep-ex/0401008
50. M. Frank, Radiative corrections to the Higgs sector of the Minimal Supersymmetric Standard Model with $\mathcal{CP}$ violation, PhD thesis, Universität Karlsruhe (Rhombos Verlag, Berlin 2003)
51. M. Frank, S. Heinemeyer, W. Hollik, G. Weiglein, hep-ph/0202166
52. A. Freitas, D. Stöckinger, Phys. Rev. D **66**, 095014 (2002), hep-ph/0205281
53. P. Azzi et al. [CDF Collaborattion, D0 Collaboration], hep-ex/0404010
54. S. Heinemeyer, W. Hollik, G. Weiglein, JHEP **0006**, 009 (2000), hep-ph/9909540
55. S. Heinemeyer, S. Kraml, W. Porod, G. Weiglein, JHEP **0309**, 075 (2003), hep-ph/0306181
56. A. Bartl, H. Eberl, K. Hidaka, T. Kon, W. Majerotto, Y. Yamada, Phys. Lett. B **402**, 303 (1997), hep-ph/9701398
57. P. Slavich, private communication
58. S. Heinemeyer, W. Hollik, G. Weiglein, Comp. Phys. Comm. **124**, 76 (2000), hep-ph/9812320; hep-ph/0002213.
The codes are accessible via www.feynhiggs.de
59. M. Frank, S. Heinemeyer, W. Hollik, G. Weiglein, hep-ph/0212037; T. Hahn, S. Heinemeyer, W. Hollik, G. Weiglein, MPP–2003–147, in Proceedings of the Physics at TeV Colliders, Les Houches, June 2003, hep-ph/0406152; in preparation